arXiv:astro-ph/0204180v1 10 Apr 2002

Photoevaporation of Clumps in Photodissociation Regions

U.Gorti and D.Hollenbach

NASA Ames Research Center, Moffett Field, CA

ABSTRACT

We present the results of an investigation of the effects of Far Ultraviolet (FUV) radiation ($6.0eV < h\nu < 13.6eV$) from hot early type OB stars on clumps in star-forming molecular clouds. Clumps in FUV-illuminated regions (or photodissociation regions or PDRs) undergo external heating and photodissociation as they are exposed to the FUV field, resulting in a loss of cold, molecular clump mass as it is converted to warm atomic gas. The heating, if rapid, creates strong photoevaporative mass flows off the clump surfaces, and drives shocks into the clumps, compressing them to high densities. The clumps lose mass on relatively short timescales. The evolution of an individual clump is found to be sensitive to three dimensionless parameters: η_{c0}, the ratio of the initial column density of the clump to the column $N_0 \sim 10^{21}$ cm^{-2} of a warm FUV-heated surface region; ν, the ratio of the sound speed in the heated surface to that in the cold clump material; and t_{FUV}/t_c, the ratio of the "turn-on time" t_{FUV} of the heating flux on a clump to its initial sound crossing-time t_c. The evolution also depends on whether a confining interclump medium exists, or whether the interclump region has negligible pressure, as is the case for turbulence-generated clumps. In this paper, we use spherical 1-D numerical hydrodynamic models as well as approximate analytical models to study the dependence of clump photoevaporation on the physical parameters of the clump, and to derive the dynamical evolution, mass loss rates and photoevaporative timescales of a clump for a variety of astrophysical situations. Turbulent clumps evolve so that their column densities are equal to a critical value determined by the local FUV field, and typically have short photoevaporation timescales, $\sim 10^{4-5}$ years for a 1 M$_\odot$ clump in a typical star-forming region ($\eta_{c0} = 10, \nu = 10$). Clumps with insufficient magnetic pressure support, and in strong FUV fields may be driven to collapse by the compressional effect of converging shock waves. We also estimate the rocket effect on photoevaporating clumps and find that it is significant only for the smallest clumps, with sizes much less than the extent of the PDR itself. Clumps that are confined by an interclump medium may either get completely photoevaporated, or may preserve a shielded core with a warm, dissociated, protective shell that

absorbs the incident FUV flux. We compare our results with observations of some well-studied PDRs: the Orion Bar, M17SW, NGC 2023 and the Rosette Nebula. The data are consistent with both interpretations of clump origin, turbulence and pressure confinement, with a slight indication for favouring the turbulent model for clumps over pressure-confined clumps.

Subject headings: ISM:clouds – ISM:dynamics – stars:early-type – stars:formation – ultraviolet:stars

1. Introduction

Young massive OB stars significantly influence the structure, dynamics, chemistry and thermal balance of their associated molecular clouds through the impact of their ultraviolet photons. Their extreme ultraviolet photons (EUV, $h\nu > 13.6$ eV) ionize the gas immediately surrounding them, forming H II regions. Far ultraviolet photons (FUV, 6 eV $< h\nu <$ 13.6 eV) dissociate molecular gas beyond the H II region, creating a photodissociation region or PDR (Hollenbach & Tielens 1999). PDRs are ubiquitous: FUV photons dominate the gas heating in PDRs and affect the chemistry and physics of gas over a large fraction of the volume and mass of molecular clouds. The study of interactions between FUV radiation and molecular cloud gas is therefore important in understanding molecular cloud evolution and the feedback between massive star formation and subsequent star formation in molecular clouds.

Observations of PDRs compared with theoretical models probe the physical conditions in star-forming regions through dust and gas emission mainly in the infrared (IR) wavelength region of the spectrum. PDRs are the source of most of the IR emission in the Galaxy. Dust grains and large carbonaceous molecules such as polycyclic aromatic hydrocarbons (PAHs) absorb radiation from the stars, and re-radiate this energy flux in the infrared, producing a continuum with solid state and PAH spectral signatures. FUV photons incident on dust grains and PAHs also cause photoelectric ejection of electrons which then collisionally heat the gas, a process called the grain photoelectric heating mechanism (e.g., Watson 1972, Bakes & Tielens 1994, Weingartner & Draine 2001). The gas cools via emission in many IR lines. Emission from PDRs has been quite successfully modelled (see Hollenbach & Tielens 1999 and references therein). The models are usually parameterized by G_0, the ratio of the FUV flux to the Habing (1968) FUV band flux of 1.6×10^{-3} erg cm^{-2}s^{-1} characteristic of the local interstellar radiation field, and n, the density of the gas. For advecting (non-stationary) models, the flow velocity of the material through the PDR is also a parameter. The FUV fields in PDRs near OB star-forming regions such as the Orion Bar or M17 SW are typically

very high, ($G_0 \sim 10^{4-5}$); the PDR gas in these regions is inferred to be very dense with average densities $\langle n \rangle \sim 10^{4-5}$ cm^{-3} (Tielens & Hollenbach 1985b). On larger scales and in more evolved regions such as the Rosette Nebula, the FUV fields and the average densities may be significantly lower by factors of $10^2 - 10^3$.

Infrared, sub-millimeter and millimeter wavelength observations of PDRs indicate that gas in PDRs is inhomogeneous (van der Werf et al. 1993, Luhman et al. 1998), which is not surprising since molecular clouds themselves are observed to be highly inhomogeneous on a wide range of scales from tens of parsecs down to tenths of a parsec (e.g., Genzel 1991). There is both indirect and direct evidence for clumpiness in PDRs. Spatially extended fine structure line emission of neutral and singly-ionized carbon near H II regions shows that the FUV penetrates deeper into the cloud than predicted by homogeneous models, suggesting that the gas is clumpy in nature (Meixner et al. 1992, Stutzki et al. 1988, Steiman-Cameron et al. 1997). Further, strengths of high excitation lines of molecular species like CO J=14→13 are observed to be greater than that predicted to arise from gas with density inferred from other PDR species. It is thus inferred that in regions such as M17 SW and the Orion Bar, the PDR gas consists of a "low" density (typically $\sim 10^{3-5}$cm^{-3}) component responsible for the extended CI and CII emission and high-density clumps (n $\sim 10^{6-7}$ cm^{-3}) which give rise to the high excitation CO lines from their surfaces or, more precisely, at a depth of $A_v \sim$1 from their surfaces (Burton et al. 1990, Meixner et al. 1992, Steiman-Cameron et al. 1997, Hogerheijde et al. 1995). Clumps are also observed directly by mapping PDRs at high spatial resolution in the 2 μm lines of H_2 (e.g., Orion Bar, Luhman et al. 1998; Eagle Nebula, Allen et al. 1999). The small regions of enhanced emission are interpreted as indicating the presence of high density clumps ($n \sim 10^{6-7}$ cm^{-3}) with sizes ≤ 0.02 pc, occupying a very small volume filling factor $\sim 1 - 2\%$. However, this interpretation is not very conclusive, and in this paper we present evidence to show that small clumps with such high densities may not exist in PDRs. Small differences in temperature within the observed regions can also explain the observed emission, as H_2 emission is highly sensitive to gas temperature (Marconi et al. 1998).

Dense PDRs like the Orion Bar are spatially thin structures and if these PDRs are indeed clumpy, the clumps must have sizes smaller than the thickness of the warm PDR, ~ 0.03 pc for the Orion Bar. The presence of small clumps affects the infrared spectrum from PDRs by introducing a range of densities in the FUV-illuminated region and by introducing enhanced advection in clumps that are photoevaporating. One of the goals of this paper is to investigate the conditions under which small, high-density clumps exist in PDRs.

Small clumps might not exist in significant numbers if the intense FUV field photoevaporates them quickly. The incident FUV field heats up and pressurizes the surface layers

of the clumps, causing the layers to expand. This mass loss may cause a complete photoevaporation of the dense clumps, and thus destroy them on short timescales. The mass loss timescales due to photoevaporation of an FUV-exposed clump can be estimated by assuming that the heated gas at the surface flows outwards at its sound speed, c_{PDR}. The mass density at the base of this heated flow, ρ_b, is lower than the mass density, ρ_c, in the cold clump, as we will discuss below. (See Table 1 for a list of frequently used symbols in this paper.) The mass loss rate is given by $dm_c/dt \sim 4\pi r_c^2 \rho_b c_{PDR}$ and since $m_c \sim \rho_c r_c^3$, the photoevaporation timescale is $t_{PE} \sim m_c/(dm_c/dt) \sim r_c \rho_c/(c_{PDR}\rho_b)$. For a typical clump, and an FUV-heated surface at 1000K, this is approximately $3 \times 10^3 (r_c/0.01\mathrm{pc})(\rho_c/\rho_b)$ years. Asymmetric mass loss from the surfaces of very small clumps can rocket them (e.g., Oort & Spitzer 1955) out of the PDR back into the cloud. Clumps that survive the rocket effect and remain in the PDR are likely to lose significant fractions of their mass on short timescales of order $\lesssim 10^{4-5}$ years, depending on the ratio ρ_c/ρ_b. The clump evaporation timescale can be longer or shorter than its residence time in the FUV-illuminated surface region of a GMC. From a frame of reference moving with the advancing ionization front, interclump material and the clumps in the GMC are advected into the PDR and ultimately flow into the H II region. Large clumps survive and they can penetrate the H II region and affect its evolution and structure, becoming Evaporating Gaseous Globules or "EGGs" (Bertoldi & McKee 1990).

In the present paper, we focus on the heating of an individual clump in a PDR by FUV photons from a nearby O or B star. We study a range of FUV fluxes incident on a range of clump sizes and determine the photoevaporative lifetimes of the clumps and the evolution of their structure. Our investigation is analogous to the study by Bertoldi (1989) and Bertoldi and McKee (1990) on the effects of EUV heating of clumps in H II regions, and a generalization of the studies by Johnstone et al. (1998) and Störzer & Hollenbach (1999) of the evaporation of small clumps and protoplanetary disks ("proplyds", O'Dell et al. 1993) by EUV and FUV photons.

In a subsequent paper (Gorti & Hollenbach, in preparation) we will discuss the cumulative effect of O and B stars on Giant Molecular Clouds (GMCs), and the relative importance of EUV and FUV photons in dissociating and destroying GMCs. Ultimately, we are interested in the role of FUV radiation in regulating star-formation in GMCs. Destruction through photodissociation and photoevaporation of potentially star-forming clumps/cores in GMCs reduces the star-forming efficiency of GMCs, and the FUV field may thereby play an important role in regulating or limiting star formation. Photoevaporation of the outer envelope of a collapsing isothermal sphere by FUV radiation could rapidly deplete the material in the envelope, and may limit the final mass of the star formed. On the other hand, compression of non-collapsing clumps by shock waves driven by the warm surface gas could possibly drive the inner cores to instability and gravitational collapse, triggering star formation.

In §2 of this paper, we discuss the present understanding of GMC structure and existing models. In §3, we describe the evolution of an H II region and its surrounding PDR as they propagate into the GMC. Timescales relevant for the FUV heating of a clump in various contexts are briefly discussed in §4. In §5 we present a simple analytical model which provides an understanding of the underlying physics of FUV-induced clump evolution. We consider various possible evolutionary scenarios and their dependences on clump parameters and the strength of the FUV field. For the more general case, a 1-D numerical hydrodynamics code has been developed and these results are described (§6). In §7, we estimate the significance of the rocket effect due to asymmetric mass loss and its effect on clump lifetimes in the PDR, and in §8 we discuss the implications of our results for observations of PDRs in star-forming regions. Application to observed PDRs is made in §9. We conclude with a summary of the present investigation (§10)

Table 1: List of symbols frequently used in this paper

Symbol	Meaning
c_c	Thermal sound speed in cold clump gas
c_{PDR}	Sound speed of heated, warm PDR gas
G_0	Strength of the FUV field in Habing units, 1.6×10^{-3} erg s^{-1} cm^{-2}
N_0	Fiducial column density equal to 2×10^{21} cm^{-2}
n_{c0}	Initial gas number density of clump
m_{c0}	Initial mass of clump
r_{c0}	Initial radius of clump
t_c	Sound crossing time in cold clump gas, r_{c0}/c_c
t_e	Expansion timescale for clumps with $\eta_{c0} > \eta_{crit}$
t_{FUV}	Timescale on which the cold clump gas gets heated to the maximum temperature in a given FUV field
t_{PE}	Photoevaporation timescale
t_s	Shock-compression timescale for clumps with $\eta_{c0} < \eta_{crit}$
v_{IF}	Velocity of the Ionization Front moving into the GMC
X_{PDR}	Thickness of the PDR in the interclump medium of the GMC, bounded by the IF and DF
α	Initial ratio of turbulent to thermal pressures in the cold clump gas
β	Initial ratio of magnetic to thermal pressures in the cold clump gas
γ	Power law exponent of the variation of density with magnetic pressure
δ_0	Initial thickness of PDR shell on the surface of a clump ($= N_0/n_{c0}$)
η_{cr}	Critical column density for complete photoevaporation of pressure-confined clumps
η_{c0}	Normalized initial column density to centre of clump, $n_{c0}r_{c0}/N_0$
η_{crit}	Critical column density in a given FUV field towards which unconfined clumps evolve
η_f	Final column density of pressure-confined clumps in an FUV field
λ	Photoevaporation parameter, $(1+\alpha+\beta)(\eta_{c0}-1)/(2(2\nu^2+\alpha))$; $\lambda = 1$ for $\eta = \eta_{crit}$
ν	Ratio of sound speeds in warm and cold gas, c_{PDR}/c_c

2. Clumps in Giant Molecular Clouds

Giant Molecular Clouds are observed to have a hierarchical substructure that is highly inhomogeneous, with density enhancements such as cores, clumps and filaments on all observable scales, from ~ 100 pc down to ~ 0.1 pc. We use the term " massive cores" to denote large scale density enhancements ($\gtrsim 1$ pc in size) and "clumps" to denote smaller scale structures ($\sim$ few tenths of pc or less in size)[1]. GMCs and their more massive constituent cores are strongly self-gravitating, and are supported against collapse by turbulence and magnetic fields. The internal velocity dispersions of the substructures in molecular clouds are found to scale with their sizes, with decreasing non-thermal support on the smallest scales (Goodman et al. 1998). The column density through a GMC or a typical GMC substructure is found to be approximately a constant $N \sim 10^{22}$ cm^{-2}, although significant variations ($N \sim 10^{21-23}$ cm^{-2}) about this typical column may occur. (For a recent review on GMCs, see McKee 1999).

The smaller substructures or clumps are not all gravitationally bound and the exact physical nature of these clumps remains uncertain (Williams et al. 2000). They have been interpreted as temporary fluctuations in density caused by supersonic turbulence within the cloud (e.g., Falgarone & Phillips 1990, Scalo 1990). This view is supported by their apparent fractal nature, which seems to show the same structure on smaller scales down to a few tenths of a parsec (Elmegreen 1999), and their observed supersonic linewidths (Blitz & Stark 1986). In this picture, the gravitationally unbound clumps are transient objects formed by converging supersonic turbulent flows. The non-gravitating clumps are therefore being constantly formed and destroyed, and have short lifetimes of the order of their sound crossing time, $t_c \approx r_{c0}/c_c$, where c_c is the clump sound speed, and r_{c0} is the initial clump radius. The effect of the sudden turn-on of an FUV field on such clumps is to drive a shock into the clump, producing a smaller, denser clump with a warm evaporative outflow. Surprisingly, the evaporative timescale is now somewhat longer than t_c, as we will show. Assuming that the FUV flux does not strongly affect the turbulence so that the formation timescale remains the same, the presence of an FUV field will not greatly change the non-gravitationally bound clump abundance, but it will compress them and alter their thermal structure and dynamical evolution.

Another interpretation is that small bound clumps as well as small unbound clumps

[1]Note that our terminology of cloud substructure is the reverse of what is sometimes used in the literature. We call the large scale structures " massive cores" and the small scale structures "clumps" to be consistent with observational work on dense regions in PDRs, wherein the density enhancements are usually called "clumps". Our notation is also consistent with the notion of "hot cores", where massive stars form.

represent stable physical entities confined by interclump pressure. Observations through molecular line spatial maps and velocity channel maps or position-velocity diagrams indicate the presence of dense coherent structures. Indirect evidence suggests the presence of a low density ($\sim 1-2$ orders of magnitude less than the clumps) "interclump medium" (ICM) (see Williams et al. 1995 and references therein). The ICM exhibits high velocity motions ($\Delta v \approx 10$ km s^{-1}) and therefore may have significant pressure, which could be of thermal, magnetic or turbulent origin. Clumps in this picture are confined by the ICM, and some of them may be self-gravitating (Maloney 1988, Bertoldi & McKee 1992). Pressure-confined clumps live much longer and presumably form more slowly than the gravitationally unbound clumps of the turbulent model. Therefore, FUV heating of these clumps and their destruction through photoevaporation will have a much more pronounced effect on lowering the clump abundance in this interpretation.

3. The Overall Evolution Of A Massive Star Forming Region

Massive stars form in the central regions of clumpy, massive, cores ($M \gtrsim 1000 M_\odot$), of radius ~ 1 pc inside GMCs (see review by Evans 1999). These massive cores contain clumps whose densities may reach $n_c \sim 10^{5-7}$ cm^{-3}, or even higher (Plume et al 1997), and the clumps are surrounded by interclump gas with lower, but uncertain densities, possibly $n_{ICM} \sim 10^{3-5}$ cm^{-3}. When a massive star forms, the EUV photons from the star immediately ionize the nearby interclump gas, and form an H II region. The clumps in the H II region are also exposed to the ionizing radiation and evaporate (Bertoldi 1989, Bertoldi and McKee 1990). The FUV photons penetrate further through the interclump gas beyond the interclump ionization front (IF) and dissociate the molecular gas, forming a dissociation front (DF) and a PDR.

In the earliest stages of evolution when EUV photons emerge from the forming O/B star, the IF moves as an R-type front. However, the IF quickly stalls and becomes D-type, at which point the high pressure H II region drives a ~ 10 km s^{-1} shock into the neutral interclump gas beyond the IF. It is instructive to obtain a sense of sizescale at the R/D type transition. Assuming the massive star emits ϕ_i Lyman continuum photons per second, the Strömgren radius at this juncture is $r_s \approx 0.1 \phi_{49}^{1/3} n_{e4}^{-2/3}$pc, where $\phi_{49} = \phi_i / 10^{49}$s^{-1} and the electron number density $n_{e4} = n_e / 10^4$ cm^{-3}. If the central star has an FUV luminosity of $L_{FUV} = 10^5 L_\odot$ (typical of stars with $\phi_{49} \approx 1$), the FUV flux incident on the surrounding PDR is characterized by $G_0 \approx 10^5$. The thickness of the PDR is approximately 10^{22}cm$^{-2}/n_{ICM}$ or $0.3 n_{ICM4}^{-1}$ pc. The DF initially advances ahead of the shock, but as photodissociation approaches equilibrium with H_2 formation, the DF slows down. Eventually, the shock moves

ahead of the DF, and the entire PDR is contained in the post-shock shell. The shock now impacts cold molecular interclump gas. Hill & Hollenbach (1978) showed that at this stage the shock velocity has slowed to $\lesssim$ 3km s^{-1}, and that, if $n_{ICM} \gtrsim 10^4$ cm^{-3}, the shock completely stalls in $t \lesssim 10^5$ years. Therefore, there is an initial stage ($t \lesssim 10^5$ years, for dense ICM) in the evolution of the clumpy PDRs surrounding H II regions where the clumps are both shocked and exposed to the photoevaporating effects of the FUV radiation. This can be followed by a stage where the shock has stalled and unshocked clumps move into the FUV-illuminated zone.

Two configurations are possible after the shock stalls. If the H II region is still completely embedded, it becomes stationary with its pressure matched by the molecular cloud pressure and the ionizing photons completely absorbed by recombining electron/proton pairs in the H II region. Much more likely is the situation where the H II region breaks through the surface of the cloud and becomes a "blister" H II region. In this case, the ionized gas can expand away from the cloud, and into the interstellar medium. The IF then slowly eats its way into the PDR and the DF similarly advances into the molecular cloud. The velocity of the IF advancing into the PDR is of order $v_{IF} \sim 1$ km s^{-1}, just enough so that the flux of particles through the IF can balance the heavily attenuated flux of EUV photons reaching the IF (see Whitworth 1979, Bertoldi & Draine 1996, Störzer & Hollenbach 1998). In such a case, the clumps entering the PDR may not have been previously shocked and compressed. Further, in the turbulent GMC model, clumps form and dissipate continually and those formed in the PDR after the passage of the shock are not affected by it. In both the PDR around the Trapezium stars in Orion and in the M17 SW PDR (Meixner et al. 1992), there is no evidence for velocity shifts between PDR gas and the ambient cloud gas, or, in other words, no evidence for a shock at the present time. In this paper, we focus only on the photoevaporation of clumps, whether or not they have been shocked, and do not follow the potential shredding or flattening of a clump by the passage of a shock wave (see, e.g. Klein et al. 1994).

The thickness or column depth of a PDR has been defined by Tielens & Hollenbach (1985) to include all the gas and dust where FUV photons play a significant role in the gas heating or chemistry. By this definition, in regions like Orion or M17, the PDR extends to columns of $\sim 10^{22}$ cm^{-2} and includes gas which is cool and molecular (H_2, CO), but where FUV still photodissociates O_2 and H_2O. We are interested in the surface column N_0 of the PDR which is heated to the highest temperatures ($T_{max} \sim 100 - 3000$K, depending on G_0 and n). For $G_0/n > 4 \times 10^{-2}$ cm^3, $N_0 \approx 1 - 3 \times 10^{21}$ cm^{-2} (equivalent to a dust FUV optical depth of order unity) and is nearly equal to the column where atomic hydrogen converts to H_2 in stationary PDRs (Tielens & Hollenbach 1985). We shall call this region the "warm PDR" hereafter to distinguish it from the entire PDR. The thickness of the warm

PDR, N_0/n_{ICM}, is of order $0.03 - 0.1 n_{ICM4}^{-1}$ pc. The crossing timescale for the IF through the warm PDR is $t_{PDR} \approx 0.3 - 1 \times 10^5 n_{ICM4}^{-1} v_{f5}^{-1}$ years, where $v_{f5} = v_{IF}/(1 \text{ km s}^{-1})$. Gas and dust (and clumps) from the opaque molecular cloud interior are therefore advected on these timescales from the shielded cloud, through the warm PDR, and across the IF into the H II region. Figure 1 shows a schematic diagram of FUV radiation from nearby O/B stars impinging on massive cores (large sizescales, e.g., Rosette) and clumps (small scales, e.g., Orion).

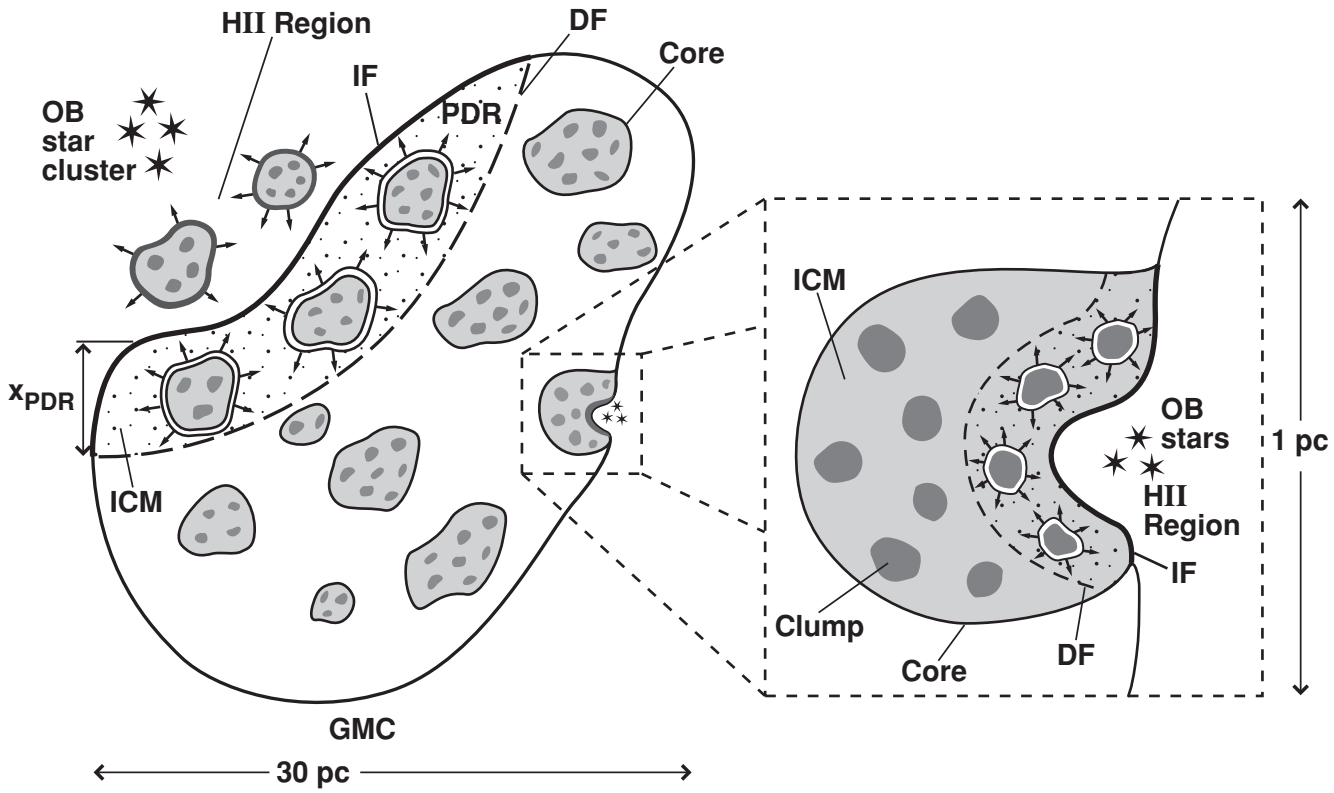

Fig. 1.— A schematic diagram of PDRs on large scales (e.g. Rosette) and small scales (e.g. Orion Bar). The figure shows blister H II regions formed by the massive stars, and the PDR bounded by the ionization and dissociation fronts. Clumps in the PDR are exposed to FUV radiation and lose mass by photodissociation and/or photoevaporation.

4. Impulsive heating versus slow heating

FUV-illuminated clumps are heated at their surfaces on timescales t_{FUV} that could be either fast or slow compared to the internal sound crossing timescale within the clump, $t_c = r_{c0}/c_c$. Impulsive heating implies that the FUV heating of the clump surface layer, characterized by column N_0, occurs with $t_{FUV} \ll t_c$. In this case, the outer region is heated more quickly than the entire clump can respond, and attains a much higher pressure than the cold central region. A shock propagates inward and a heated photoevaporative flow expands off the surface.

Several situations in clumpy molecular clouds may lead to $t_{FUV} \ll t_c$. For a clump with $r_{c0} \sim 10^{17}$ cm and $c_c \sim 0.3$ km s^{-1} (T $\sim$ 10K), $t_c \sim 10^5$ years. The OB star may "turn-on" on a timescale $< 10^5$ years. Even after this initial flash of FUV flux, the clumps may shadow each other so that t_{FUV} is given by the time for a clump to move out of shadow, which is of order r_{c0}/v_c, where v_c is the clump velocity. In a turbulent, supersonic medium v_c may be larger than c_c so that $t_{FUV} < t_c$. Similarly, if clumps are formed in turbulent gas by supersonic converging flows, the FUV turn-on timescale is roughly the time for the clump to form, which again is $t_{FUV} \approx r_{c0}/v_t$, where v_t is the supersonic turbulent speed. Therefore, impulsive heating is likely the most appropriate approximation for the turbulent model of clumps in molecular gas.

Let us consider the other situation of long-lived clumps confined by the ICM. Here, slow heating is generally the best approximation, but in certain conditions, impulsive heating may be more appropriate. A common situation after the turn-on of the OB star may be the advancement of the ionization front and PDR front into the opaque molecular cloud, which occurs at speeds $v_{IF} \sim 1$ km s^{-1}. In this situation t_{FUV} is the time for the DF and the IF to move so that the clump is one FUV optical depth closer to the IF, or $t_{FUV} \approx t_{PDR} = X_{PDR}/v_{IF}$, where $X_{PDR} = N_0/n_{ICM}$ is the thickness of the heated PDR zone in the ICM of density n_{ICM}. The criterion for impulsive heating $t_{FUV} < t_c$, is more easily met by larger clumps that have longer sound crossing timescales, as t_{FUV} is the same for all clumps. This gives us a limiting size for clumps likely to be impulsively heated,

$$r_{c0} > X_{PDR}\frac{c_c}{v_{IF}} \approx (0.3-1)X_{PDR}, \tag{1}$$

which is of the order of the thickness of the interclump PDR region itself. Clumps with radii smaller than this are slowly heated as they emerge from the opaque molecular cloud into the FUV-irradiated regions. Since we only consider clumps *within* PDRs that have $r_{c0} < X_{PDR}$, pressure-confined clumps are generally slowly heated in our analysis.

Clumps that undergo slow heating, $t_{FUV} \gg t_c$, adjust quasi-statically to the changing FUV flux. Long-lived, small, pressure-confined clumps advecting into FUV-irradiated regions

provide a prime example of this slow evolution. Such clumps develop a warm PDR surface which slowly gets warmer, thicker and less dense. The clump and the heated PDR surface evolve in near pressure equilibrium, with the density of the surface decreasing with the rise in its temperature, such that $n_{PDR}T_{PDR} = n_cT_c$ = pressure of the ICM (assuming thermal pressure dominates on these small scales). At any given time, the evolutionary state of a slowly heated clump is the same as the *final* state of an impulsively heated clump exposed to the same local FUV flux. However, a gradually heated clump constantly adjusts its PDR surface to maintain pressure equilibrium as the PDR slowly heats. In contrast, an impulsively heated clump undergoes shocks and supersonic expanding flows in its attempt to attain equilibrium. (We note that there is no final equilibrium state if the interclump pressure is zero). Rapid photoevaporative mass loss can cause an acceleration due to a rocket effect in very small clumps and move them back into the shielded cloud. Pressure-confined small clumps, on the other hand, are not rocketed as they evolve quasi-statically. In a given FUV field and at a given ICM pressure, the final equilibrium state of a small clump is either a completely photodissociated, warm (T_{PDR}), and expanded (but with $P = P_{ICM}$) region; or it may consist of a shielded cold molecular core with the same temperature, density and pressure as the original clump, but with a heated and more diffuse protective surface layer of PDR material. In §5.3 we provide analytic solutions for these equilibrium structures. However, in §5 and §7 we primarily focus on the interesting physical processes which occur for clumps that are impulsively heated.

5. Analytical models for FUV photoevaporating clumps

We first provide approximate analytic solutions for the time evolution of a clump suddenly exposed to FUV radiation, using a few simplifying assumptions. As described in §2, the nature of the clumps themselves is not well understood, and we consider two simple analytic models that qualitatively correspond to the two main interpretations. Turbulent unbound clumps are modelled as constant density structures in vacuum. A clump in vacuum disperses on a sound crossing timescale, in the absence of FUV illumination. Pressure-confined clumps are also treated as being of constant density, but have a surrounding ICM with equal pressure. In our models, the ICM only serves to confine the clumps and does not itself evolve or otherwise affect the clump evolution. We seek solutions for the time evolution of the mass, size and mass loss rate of a photoevaporating clump.

5.1. Initial conditions and assumptions

Clumps are assumed to be dense, small spheres of gas, supported by thermal, turbulent and magnetic pressures. We assume that the magnetic field B scales with a constant power of the density, so that the magnetic pressure is

$$P_B = B^2/8\pi \propto n^\gamma. \tag{2}$$

The initial ratio of turbulent and magnetic pressures, P_{NT} and P_B, are set by two dimensionless parameters,

$$\alpha = P_{NT}/P_T; \qquad \beta = P_B/P_T \tag{3}$$

where P_T is the initial thermal gas pressure in the clump. A clump may have significant turbulent support and observations of clumps in star-forming regions (Jijina et al. 1999) indicate values of α ranging from ~ 0 in cold, dark clouds to $\gtrsim 2$ in regions of massive star formation. There is observational evidence to suggest that turbulent support in clumps decreases on the smaller scales of star-forming clumps ($r_{c0} \lesssim 0.1$ pc), where $\alpha \lesssim 1$ (Goodman et al. 1998). Measurements of magnetic fields and hence β and γ are difficult, but present observational data suggest a wide range of values for β, from ~ 0 to a few (Crutcher 1999). The value of γ ($\sim 1-2$) describes how the B field responds to a relatively sudden change in gas density. For a frozen, uniform magnetic field threading a spherical clump, $B \propto n^{2/3}$ or $\gamma = 4/3$. For our standard case we adopt values of $\alpha = 1, \beta = 1$, and $\gamma = 4/3$. We later discuss the sensitivity of our results to these choices for α, β and γ. As discussed in §4, for clumps confined by an ICM and advecting into FUV-illuminated interclump zones, the assumption of $t_{FUV}/t_c < 1$ is equivalent to $r_{c0} \gtrsim (0.3-1)X_{PDR}$. Therefore, in this case we treat only clumps above a certain minimum size, which is of order the size of the thickness of the heated PDR of the ICM. We do not explicitly include self-gravity in our analytical model, and only qualitatively estimate the effects of gravity on clump evolution. We treat gravity more quantitatively in the numerical models.

The FUV radiation field as seen by the clump is spherically asymmetric, and stronger at the surface facing the source. For simplicity, however, we assume a spherically symmetric FUV field when calculating the internal dynamical evolution and the thermal structure of the evaporating clump. Typical albedos of interstellar dust are ~ 0.5 and some of this scattered radiation is directed backwards (dependent on the phase factor g, see Henyey & Greenstein 1941), resulting in a backscattered FUV flux on the shielded clump surface about $0.1-0.2$ times that on the directly illuminated surface (e.g., Désert et al. 1990, Hurwitz et al. 1991). Although the posterior intensity is diminished compared to that on the front surface, the PDR surface sound speed is not a sensitive function of the incident FUV flux G_0 (Kaufman et al. 1999). For field strengths $G_0 \sim 10^{3-5}$ near typical H II regions and densities $n \gtrsim 10^{3-6}$

cm^{-3} characteristic of clumps there, even a back flux 10% of that on the clump surface facing the source would heat the gas to nearly the same sound speed (c_{PDR} = 3 km s^{-1} on the source side, c_{PDR} = 2 km s^{-1} on the shadowed side). Therefore, the assumption of spherical symmetry is as good as ignoring the flux of FUV photons on the backside when calculating the thermal structure and internal dynamics. However, the asymmetry of the flows from the front and back surface will cause a rocket effect on the clumps and induce motion away from the source, as first recognized by Oort & Spitzer (1955). We discuss momentum transfer due to mass loss of the clumps in §7, and estimate sizes of clumps that gain velocities high enough to move out of the PDR and back into the molecular cloud.

In our analytical models (but not our numerical models) we assume that the transition from the warm outer PDR layer to the cold molecular core of a clump is very thin, so that the clump can be modelled as an isothermal core with sound speed c_c, surrounded by a PDR envelope of sound speed c_{PDR}. The gas in the core always remains isothermal in our analysis, even when shock-compressed to high densities. For our pressure-confined clumps, it is assumed that the ICM is of low density and does not absorb any FUV photons. In order to obtain analytic solutions, we do not fully treat transient phenomena and emphasise quasi-steady state aspects of the flow.

5.2. Analytic model for unconfined clumps

We begin by considering the evolution of a simple configuration: a cloud consisting of clumps that are spheres of radius r_{c0} and constant initial density n_{c0}, immersed in a vacuum. We refer to such clumps hereafter as "turbulent clumps". These are dynamic structures that in the absence of FUV heating expand at roughly their sound speed, c_c. When such a clump is exposed to an FUV field, the photon flux is attenuated by dust and instantaneously heats an outer column of $N_0 \sim 2 \times 10^{21}$ cm^{-2} (thickness $\delta_0 = N_0/n_{c0}$) to relatively high temperatures and sound speeds (for example, near H II regions with $G_0 \sim 10^{4-5}$ and $n_{c0} \sim 10^5$ cm^{-3}, $T \sim 1000$K and $c_{PDR} \sim 3$ km s^{-1}).

The evolution of the clump is determined by its initial radial column density from the centre outwards, $n_{c0}r_{c0}$, and the ratio ν of sound speeds in the FUV-heated region and the cold clump material,

$$\nu = c_{PDR}/c_c \tag{4}$$

The parameter ν can be thought of as a measure of the strength of the FUV field incident upon the cold clump. We introduce the dimensionless parameter η_{c0},

$$\eta_{c0} = n_{c0}r_{c0}/N_0 = r_{c0}/\delta_0, \tag{5}$$

for the initial column density to the centre of the clump. Note that η_{c0} is a measure of the mean column density through a clump.

For turbulent clumps with $\eta_{c0} \leq 1$, the initial clump column density is less than N_0, and the entire clump is immediately heated and photodissociated by the FUV flux. Effectively, therefore, the FUV flux accelerates the expansion of the cold clump by heating it throughout, decreasing the expansion timescale by a factor given by the ratio of sound speeds at the two temperatures, c_c/c_{PDR}, or $1/\nu$. For clumps with $\eta_{c0} > 1$, the FUV flux heats an outer shell of gas to a higher temperature, thereby increasing its pressure. If the pressure of the outer PDR shell is sufficiently high, it drives a shock to the centre of the clump rapidly compressing it, and the compressed clump proceeds to evaporate on a somewhat longer timescale than the expansion timescale in the absence of an FUV field. On the other hand, if the pressure in the heated outer PDR shell is low, the shock does not make it to the centre of the clump. The shock dissipates, followed by an expansion of the clump, until finally the photoevaporative flow halts the expansion and proceeds to shrink and compress the gas. There are thus two distinct evolutionary scenarios for photoevaporating turbulent clumps with $\eta_{c0} > 1$.

For brevity in the main text, the details of our analysis and the derivations of the results are presented in the appendices to the paper. We now discuss our solutions and describe the physics of FUV-heated clump evolution and refer the interested reader to the appendices for the full analysis.

Clumps exposed to a given FUV field, measured by the parameter ν, are either compressed by shocks or expand to adjust their column density to a critical value, η_{crit}. This critical column density, η_{crit} can be derived from conservation of mass and from the condition of pressure equilibrium at the surface of the cold clump gas (see Appendix A for details), and is defined by the relation

$$\frac{2(2\nu^2+\alpha)}{\eta_{crit}-1} + \beta\left(\frac{2}{\eta_{crit}-1}\right)^{\gamma} = 1+\alpha+\beta \tag{6}$$

Recall that α and β are the initial ratios of turbulent to thermal pressure and magnetic to thermal pressure, respectively, and that the magnetic pressure scales as n^{γ}. For typical values of these parameters, the second term on the LHS is negligible and equation (6) can be used to define a photoevaporation parameter, λ, as

$$\lambda = \frac{(1+\alpha+\beta)(\eta_{c0}-1)}{2(2\nu^2+\alpha)}. \tag{7}$$

For clumps with initial column densities $\eta_{c0} = \eta_{crit}$, the photoevaporation parameter $\lambda = 1$. Figure 2 shows an $\eta - \nu$ parameter plot with equation (6) depicted for the standard case with $\alpha = 1, \beta = 1$, and $\gamma = 4/3$, and for two possible extremes of these parameters. The

result is not very sensitive to the choice of the parameter γ, and η_{crit} only depends on the sum of α and β. For the standard case and with $\eta_{c0} \gg 1$ and $\nu \gg 1$ which is typical of many PDRs, equation (6) can be approximated as $\eta_{crit} \approx 4\nu^2/3$. The evolution of FUV-heated clumps is determined by where they initially lie in the $\eta - \nu$ parameter space.

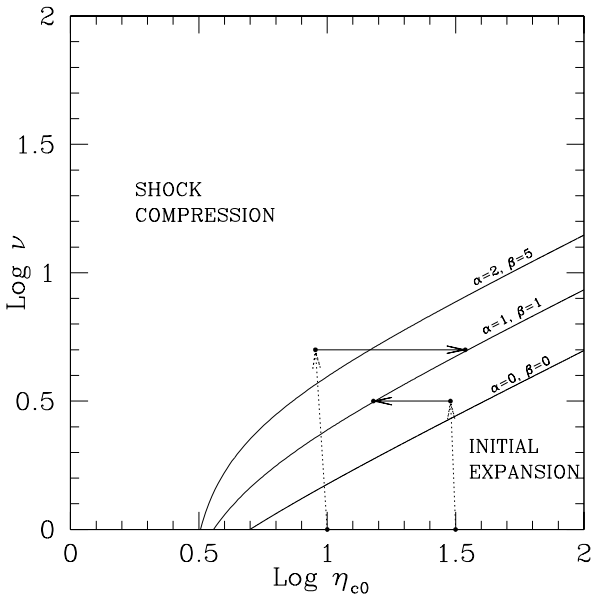

Fig. 2.— Logarithmic parameter plot of the ratio η_{c0} of the initial column density through the clump to the fiducial column N_0, and the ratio ν of the sound speed in the heated PDR gas to that in the cold clump gas, for impulsively heated clumps. The critical column density η_{crit} is plotted against ν for different values of α and β, with $\gamma = 4/3$. Also shown are representative trajectories of column density evolution for clumps with initial column densities less than, and greater than, η_{crit}. Note that, in this case, the abscissa refers to the instantaneous column density through the clump. At $t = 0$, $\nu = 1$ and the clump has a column η_{c0}. With the turn-on of the FUV field, ν increases rapidly. A clump with $\eta_{c0} < \eta_{crit}$ is then compressed by a shock to η_{crit} and moves right on this parameter plot and then proceeds to photoevaporate steadily. A clump with $\eta_{c0} > \eta_{crit}$ expands so that its column density becomes equal to η_{crit} and continues to photoevaporate. The initial turn-on of the FUV field (dotted line) moves the column slightly to the left because a column N_0 is quickly dissociated and lost from the clump. Gravity is ignored in this figure (see Figure 5).

Clumps with an initial column density $\eta_{c0} < \eta_{crit}$ evolve through a shock-compression phase, until their dimensionless column density increases to η_{crit} (see Appendix B). Clumps with higher initial column densities expand until their column density decreases to η_{crit} (see Appendix C). The evolution of clumps in two representative cases is qualitatively shown in Figure 2 through their trajectories in $\eta - \nu$ space. Once the clump column density attains its critical value η_{crit}, further evolution is similar in both cases, and the clump column density at any later time remains constant at this critical value. We note that this would imply that observed clumps in a given PDR should typically have the same column density, the critical value η_{crit} given by the ambient FUV field. This is valid for clumps photoevaporating into a vacuum and only violated in the transient early stages which are typically very short, of order $t \approx r_{c0}/c_{PDR}$. From equation (6), clumps at 10K heated on their surfaces to 100 K (or $\nu \sim 3$) should have columns $\eta_{crit} N_0 \sim 3 \times 10^{22}$ cm^{-2}, and for $T \sim 1000K$ or $\nu \sim 10, \eta_{crit} N_0 \sim 3 \times 10^{23}$ cm^{-2}. As photoevaporation proceeds, and clumps lose mass, they shrink in size and their average density increases, so that the column through the clump remains the same, $n_c(t) r_c(t) = \eta_{crit} N_0$.

Shock compression In this case, the initial column density is larger than N_0, but smaller than $\eta_{crit} N_0$. The FUV can only penetrate through an outer shell of thickness $\delta_0 = N_0/n_{c0} < r_{c0}$. This shell is heated to a higher temperature and the corresponding increase in pressure causes the outer shell to expand at c_{PDR} radially outwards at the edge and inwards into the clump at the inner boundary. Figure 3 shows a schematic diagram of the evolution of a shock-compressed clump.

Fig. 3.— Schematic diagram of evolution of shock-compressed clump. The cold clump is indicated by the lightly shaded region, the dotted region represents the heated warm PDR surface of the clump, and the dark shaded region shows shock-compressed gas. Panel c shows the propagation of the shock front into the clump and panel d depicts the evolution of the clump after being compressed by the shock into a small dense core.

As the shell expands, the column density N_0 through it is maintained by further penetration of FUV photons, and heating of more cold clump material. The pressure at the base of the PDR shell is initially higher than the cold clump gas. This pressure difference drives a shock wave into the clump, which rapidly propagates to the centre. Behind the shock the cold clump gas is compressed to a pressure approximately equal to the pressure at the base of the PDR shell. The shock travels inward at roughly c_{PDR} and the entire clump gets compressed in a time $t_s \simeq r_c(0)/c_{PDR}$, where $r_c(0) = r_{c0} - \delta_0$ is the initial radius of the cold clump when the FUV flux is turned on (Fig. 3b). The shock reaches the centre and compresses the clump to a radius $r_c(t_s) = r_s$. The shock-compressed gas forms a high-density core, such that the pressures in the core and at the base of the PDR flow are approximately equal. Further mass loss from the clump is from the surface of this core. The time evolution of the mass and radius of the clump for $t > t_s$ are given by the following equations for our standard case, where $\alpha = 1$, $\beta = 1$, and $\gamma = 4/3$. For the general solution, refer to Appendix B.

$$r_c(t > t_s) = \left(\left(\frac{r_s}{r_c(0)} \right)^{5/4} - \frac{10\eta_{c0}\nu}{3(\eta_{c0}-1)^2} q^{9/4} \left(\frac{t}{t_c} - \frac{(\eta_{c0}-1)}{\eta_{c0}\nu} \right) \right)^{4/5} r_c(0) \tag{8}$$

$$\frac{dm_c}{dt} = \left(\frac{m_{c0}}{t_c} \right) \left(\frac{r_c(t)}{r_{c0}} \right) \frac{6\nu}{\eta_{c0}} \tag{9}$$

$$m_c(t > t_s) = m_c(0) \left(\frac{r_c(t)}{q r_c(0)} \right)^{9/4} \tag{10}$$

Here $q = (\lambda/3)^{1/3}$, $r_s \approx q r_c(0)(1 - 3(1+q)/(\eta_{c0}-1))^{4/9}$ and $t > t_s = r_c(0)/c_{PDR}$. The PDR/core interface propagates inward as the warm gas evaporates and, finally, the entire core is transformed to heated, photodissociated, expanding PDR material. Using equations (8) and (10), Figure 4 shows the clump radius and mass as a function of time for a case where the initial column through the clump is given by $\eta_{c0} = 10$, and $\nu = 5$ represents the incident FUV flux. This is a typical column density for clumps in molecular clouds, (see §2) and for a clump of mass m_c, corresponds to a density $n_{c0} = 3 \times 10^6 (M_\odot/m_c)^{1/2}$ cm^{-3}. In this example of $\nu = 5$, the FUV field might heat cold clump gas with initial temperature of ∼30 K to about ∼750 K, or ∼ 10K gas to about 250 K.

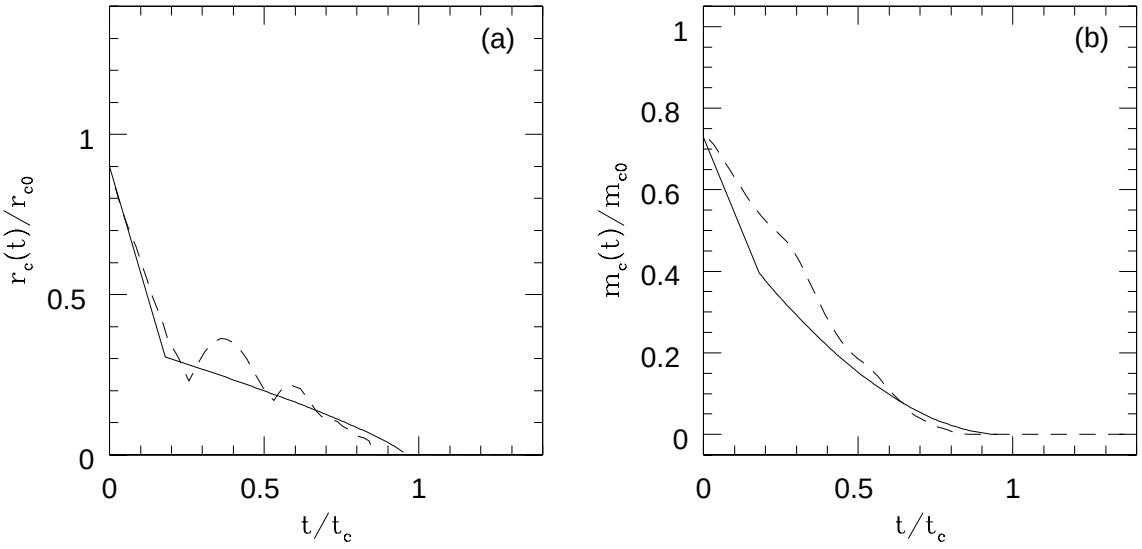

Fig. 4.— Time evolution of radius (panel a) and mass (panel b) of cold clump gas for a clump with $\eta_{c0} = 10, \nu = 5$ that undergoes shock compression. The mass and radius are given as ratios to the initial mass and radius, and time is in units of sound crossing times in the initial cold clump. The solid line is the analytical result, showing an initial rapid decrease in clump radius followed by a slower phase of clump radius evolution. The dashed line is the result from the 1-D hydrocode and is seen to agree well with the analytical curve.

Also shown in Figure 4 are the results of a more detailed hydrodynamics code simulation (described in the next section) for the same parameters. There is very good agreement between the two results, in spite of the various simplifying assumptions made in arriving at the analytical solutions. The numerical solution for $r_c(t)$ oscillates with time due to the dynamics of the shock compression which we have neglected in the above analysis. Our analytic solution assumes a quasi-steady state, whereas the numerical code shows the effect of overshooting the steady state solution and rebounding.

The clump evolution goes through two distinct phases, which is apparent from the plot of clump radius with time (Fig.[4a]). The clump initially shrinks rapidly with time, as the shock compresses the clump in a time t_s. The average velocity v_b with which the radius decreases is $0.65 c_{PDR}$ for the chosen parameters. After the entire clump is compressed by the shock, it decreases in size more slowly, now due entirely to the mass loss from its surface. As discussed earlier, the column density in the compressed clump remains constant, and the clump gets denser as its size decreases. In Figure 4b, the mass of the clump is also seen to decrease with time as the entire clump gets photoevaporated in about a sound crossing time; again, the analytical results closely follow the result of the numerical hydrodynamical code. The cold clump mass at $t = 0$ is less than the initial clump mass because it excludes the mass contained in the outer column N_0 which is instantaneously heated by the FUV flux to the PDR temperature.

Using the results of the above analysis, we can obtain simple estimates of photoevaporation timescales for a clump exposed to incident FUV radiation. We define the photoevaporation timescale, t_{PE}, as the time for the radius of the clump to shrink to zero. The time t_{PE}, can be easily determined from setting the LHS of equation (8) to zero,

$$t_{PE} \approx 0.5 \eta_{c0}^{2/3} \nu^{-1/3} t_c \tag{11}$$

or

$$t_{PE} \approx 10^4 \left(\frac{n_{c0}}{10^5 \mathrm{cm}^{-3}}\right)^{2/3} \left(\frac{r_{c0}}{0.01\mathrm{pc}}\right)^{5/3} \left(\frac{0.3\mathrm{kms}^{-1}}{c_c}\right)^{2/3} \left(\frac{3\mathrm{kms}^{-1}}{c_{PDR}}\right)^{1/3} \mathrm{years} \tag{12}$$

Larger clumps are longer-lived compared to smaller clumps in a given PDR environment. Photoevaporation timescales of turbulent clumps in PDRs in typical star-forming regions are thus of the order of a few clump sound crossing times (see §7). Paradoxically, the sudden turn-on of FUV radiation on a clump in a vacuum can increase its lifetime, even though the FUV heats the surface and increases the flow speed from the surface! For turbulent clumps with lifetimes $\sim t_c$ in the absence of an FUV field, exposure to the FUV field results in a "pressure-confined" period where the clump is compressed due to pressure of the heated surface PDR layer. This compression reduces the area of the photoevaporating surface and can extend the lifetimes of these clumps to a few t_c.

Collapse of clumps driven by shock compression The FUV driven shock wave that compresses a clump to very high densities, may render it gravitationally unstable to collapse. Thus star formation may be triggered in a previously stable clump. A simple estimate of parameters leading to clump collapse can be made without explicitly including self-gravity in the equations. We use our solutions for the radius of the shock-compressed core (Appendix B) and compare this with its Jeans length, r_J. If $r_s < r_J$, the clump is stable, otherwise it undergoes gravitational collapse. It should be noted here that a clump supported by magnetic pressure with $\gamma > 4/3$ will always be stable to collapse regardless of the external pressure, as the magnetic pressure increases faster during compression than the gravitational energy density. Our discussion here is thus applicable for clumps with insignificant magnetic fields, or with a magnetic equation of state where $\gamma \lesssim 4/3$. We now solve for the collapse criterion as a function of initial clump parameters and the FUV field strength as measured by ν, for an illustrative case where $\alpha = 1, \beta = 1$, and $\gamma = 1$. The radius of the shock-compressed core is given by

$$r_s \simeq r_c(0) \left(\frac{3(\eta_{c0} - 1)}{4(\nu^2 + 1)} \right)^{1/2} \tag{13}$$

The Jeans length of the compressed core is given by

$$r_J = \left(\frac{3\pi c_c^2}{4 G m_H n_s} \right)^{1/2} \tag{14}$$

For collapse $r_s > r_J$ which yields

$$\eta_{c0} > 1 + \frac{3}{4} \left(\frac{\pi n_{c0} c_c^2}{G m_H N_0^2} \right)^{2/3} (\nu^2 + 1)^{-1/3} \tag{15}$$

The factor $n_{c0} c_c^2$ in equation (15) is the initial thermal pressure in the clump, and for clumps in PDRs is typically of the order of 10^{6-7} cm^{-3} K. For $n_{c0} c_c^2 = 10^6$ cm^{-3} K, equation (15) becomes

$$\eta_{c0} > 1 + \frac{49}{(\nu^2 + 1)^{1/3}} \tag{16}$$

Figure 5 shows the collapse criterion(Eq.[16]) on the $\eta - \nu$ parameter plot. Clumps with initial column densities greater than $\sim 40 N_0$ and with initial thermal pressures of 10^6 cm^{-3} K cannot support themselves against gravity and are unstable to collapse even in the absence of an FUV field. This region of instability is to the right of the vertical dotted line in the plot. Clumps to the left of this line are initially stable, but sufficiently strong FUV fields may drive shocks that compress them and trigger collapse. The FUV fields near OB stars may thus trigger star formation in previously stable clumps, and *increase* the star formation rate in clouds, in cases where $\gamma < 4/3$.

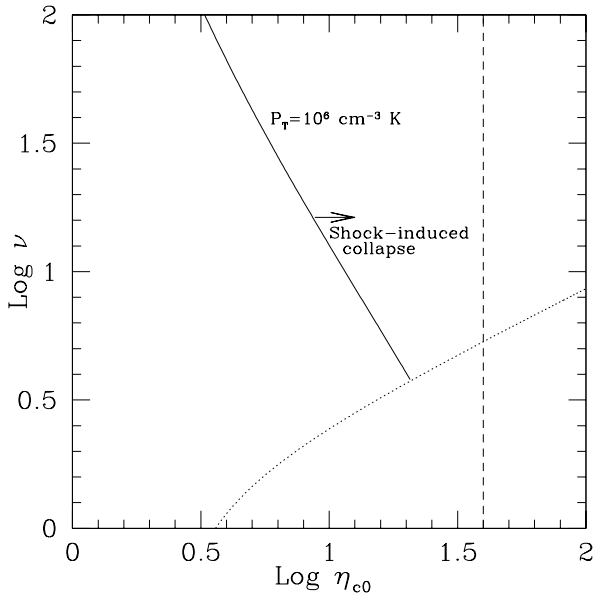

Fig. 5.— This figure shows the $\eta - \nu$ parameter space and demarcates the regions where gravitational collapse can be triggered by shock compression (for $\gamma = 1$). The dashed line indicates the column densities of clumps, with thermal pressure 10^6 cm^{-3} K, which are initially unstable to collapse. Clumps with this pressure and columns to the left of the line are initially stable. The regions to the right of the solid line are where clumps are driven to collapse by shocks induced by photoevaporation, for initial thermal pressures in the clump $P_T = 10^6$. For higher pressures P_{c0}, both the dotted ($\eta \propto P_{c0}^{1/2}$) and solid lines ($\eta \propto P_{c0}^{2/3}$) move to the right.

Clumps with an initial expansion phase Clumps with initial column densities $\eta_{c0} > \eta_{crit}$ as given by equation (6) develop very thin ($\delta_0 \ll r_{c0}$) PDR shells when they are first exposed to FUV radiation. This very thin shell is initially at a high pressure and drives a shock into the clump on the inside edge of the shell while the outside edge of the shell expands at roughly c_{PDR} just as is the case for shock-compressed clumps. However, the shock stalls before it reaches the clump centre as the PDR pressure rapidly declines due to the shell expansion. The PDR pressure and clump pressure become equal before the shell thickness is comparable to the clump radius. We summarize below the detailed evolution of initially expanding clumps; details appear in Appendix C.

Because of the high PDR sound speed and relatively small thickness, the PDR pressure initially drops faster than the pressure in the cold clump. The pressure in the cold clump eventually becomes higher than that in the surrounding expanding PDR shell, and the cold clump gas expands at its sound speed, c_c (as it would in the absence of FUV radiation since the interclump medium is assumed here to be a vacuum). This expansion takes place until a time t_e at which the density (and pressure) in the clump gas drops to that of the outer PDR layer. For $t > t_e$, FUV photons begin penetrating into the formerly shielded cold clump gas. The warm PDR gas now confines the clump gas, and further expansion of the cold clump is halted. The cold clump proceeds to lose mass gradually and shrinks due to photoevaporation, with an evolution similar to the final solution for shock-compressed clumps. The radius and mass of the clump at times $t > t_e$ and for $\alpha = 1, \beta \leq 1, \gamma \leq 4/3$ are given by

$$r_c(t > t_e) = r_c(t_e) - \frac{3c_{PDR}}{2\nu^2 + 1}(t - t_e) \tag{17}$$

where $r_c(t_e) = r_c(0) + c_c t_e$,

$$t_e = t_c \left(1 - \frac{1}{\eta_{c0}}\right) \left(\left(\frac{3\nu + \eta_{c0} - 1}{3\nu + 2\nu^2 + 1} \right)^{1/2} - 1 \right) \tag{18}$$

and

$$m_c(t > t_e) = m_{c0} \frac{(2\nu^2 + 1)}{\eta_{c0}} \left(\frac{r_c(t)}{r_{c0}} \right)^2 \tag{19}$$

Figure 6 shows the change in radius and mass of a clump with initial parameters $\eta_{c0} = 100, \nu = 3$. The clump expands out initially and loses a small fraction of its mass during this phase. After its density has dropped, so that there is pressure equilibrium between the cold clump gas and the heated layer immediately surrounding it, expansion is halted. As photoevaporation causes mass loss off its surface, the clump shrinks in size, and is completely heated and photodissociated in about 4 crossing timescales. The numerical results are also overlaid on the plot, and there is reasonable agreement. The photoevaporation timescale for

initially expanding clumps can be defined analogously to shock-compressed clumps as (see Appendix C, Eq.(C7))

$$t_{PE} \approx \frac{4}{3}\nu t_c \approx 10^5 \left(\frac{c_{PDR}}{3\mathrm{kms}^{-1}}\right)\left(\frac{0.3\mathrm{kms}^{-1}}{c_c}\right)^2\left(\frac{r_{c0}}{0.01\mathrm{pc}}\right)\mathrm{years} \tag{20}$$

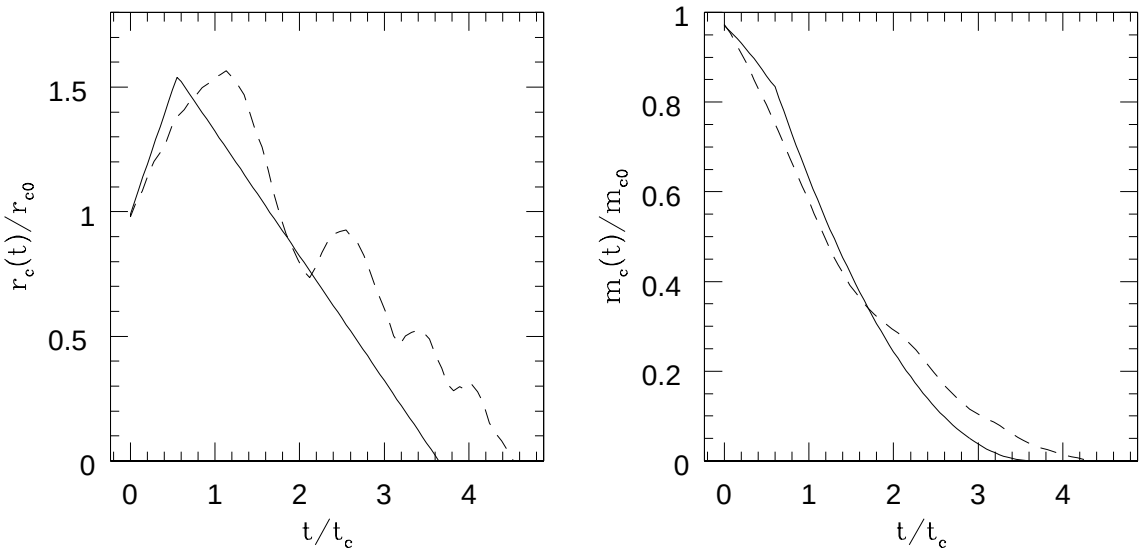

Fig. 6.— Time evolution of radius and mass for an initially expanding clump, with $\eta_{c0} = 100, \nu = 3$. Radius and mass are given as ratios of their initial values and time is in sound crossing time units, t_c. The figure shows the analytical result (solid line) and that from the numerical code (dashed line). The clump radius increases in the beginning as the clump expands and then shrinks as the clump loses mass due to photoevaporation.

Therefore in this regime of low ν, the photoevaporation timescale t_{PE} is of order several sound crossing timescales, and is proportional to ν.

5.3. Analytical model for clumps pressure-confined by an interclump medium

For a cloud model in which clumps are structures in pressure equilibrium with an ICM, the evolution of FUV-heated clumps is somewhat different. The heated shell or PDR can now no longer expand indefinitely, but is eventually confined by the pressure of the ICM. The evolution of the clump is again determined by η_{c0} and ν. Clumps with an initial column density $\eta_{c0} < N_0$, are completely heated and photodissociated instantly. Such clumps expand until the PDR gas reaches the interclump pressure. Clumps with higher initial column densities again are only heated on their surfaces to a column N_0, and their further evolution depends on the turn-on time of the FUV field t_{FUV}, relative to t_c.

If the clumps are heated impulsively, $t_{FUV} \ll t_c$, pressure-confined clumps initially evolve similarly to the turbulent clumps discussed earlier. Clumps with $\eta_{c0} < \eta_{crit}$ are thus shock-compressed, and mass flows are set up which photoevaporate the clump. However, the outflow runs up against the interclump pressure and eventually reaches pressure equilibrium with its surroundings. During this time, the clump may either be completely heated through and get transformed into a sphere of warm PDR gas, or may only be partially photoevaporated. The final configuration for partially photoevaporated clumps consists of a small remnant cold clump, and an extended warm PDR envelope surrounding it and protecting it from the FUV flux. The clump, PDR envelope and interclump medium are in pressure equilibrium. Clumps with $\eta_{c0} > \eta_{crit}$ are not much affected by the FUV field. There is no expansion of the clump due to the presence of the confining ICM, and the initially heated thin PDR shell expands to form an expanded, but still thin, protective PDR layer. Containment of the PDR shell by the ICM prevents further penetration of FUV photons into the cold clump and there is no additional heating. For these clumps, photoevaporation is relatively unimportant and they retain large fractions of their initial masses.

Clumps that are heated with $t_{FUV} > t_c$ evolve quasi-statically, steadily adjusting themselves to the pressure of the heated PDR shell. The evolution of these clumps can be determined from simple steady-state equilibrium considerations. In their final configuration, the clumps may retain a fraction of their initial cold gas, surrounded by a warm PDR envelope, in pressure equilibrium with the ICM. We consider two extremes in density profiles of the clump, a constant density clump and a truncated isothermal sphere ($n \propto 1/r^2$) in pressure equilibrium with the ICM.

First, we solve for the evolution of a clump of constant density. From conservation of mass,

$$n_{c0}{r_{c0}}^3 = n_f {r_f}^3 + n_{PDR}(r_{PDR}^3 - r_f^3) \tag{21}$$

where n_f and n_{PDR} are the number densities in the final cold clump core and the PDR, and r_{c0}, r_f, and r_{PDR} are the radii of the initial clump, remnant clump, and the PDR envelope respectively. As the final configuration is a remnant clump in pressure equilibrium with the PDR and the ICM, the final density of the core $n_f = n_{c0}$, and

$$n_{c0}{c_c}^2 + \alpha n_{c0}{c_c}^2 + \beta n_{c0}{c_c}^2 = n_{PDR}{c_{PDR}}^2 + \alpha n_{PDR}{c_c}^2 + \beta n_{c0}{c_c}^2 (n_{PDR}/n_{c0})^\gamma \text{ (= Pressure in the ICM)} \tag{22}$$

Further, we know that the column density through the PDR envelope is N_0, as the remnant clump is shielded from heating. Therefore,

$$n_{PDR}(r_{PDR} - r_f) = N_0 \tag{23}$$

Using equations (21) and (23) to eliminate n_{PDR} and r_{PDR}, equation (22) can be written as

$$\nu^2 = (1 + \alpha + \beta)\xi - \beta\xi^{1-\gamma} - \alpha \tag{24}$$

where

$$\xi = \left(\eta_{c0}^3 - \eta_f^3 - \frac{3}{4}\eta_f^2\right)^{1/2} - \frac{3}{2}\eta_f \tag{25}$$

and $\eta_f = n_{c0} r_f / N_0$. For complete photodissociation $\eta_f = 0$, or $\xi = \eta_{c0}^{3/2}$. For the standard case $\alpha = 1$, $\beta = 1$ and $\gamma = 4/3$, and for $\eta_{c0} > 1, \nu > 1$, equation (24) can be used to define a critical column density for complete photoevaporation.

$$\eta_{cr} \simeq 0.48\nu^{4/3} \tag{26}$$

All clumps with an initial column density lower than η_{cr} are thus eventually completely photodissociated. Alternately, a clump with an initial column density η_{cr} has to be exposed to an FUV field (ν) greater than or equal to that given by equation (26) to be completely photodissociated.

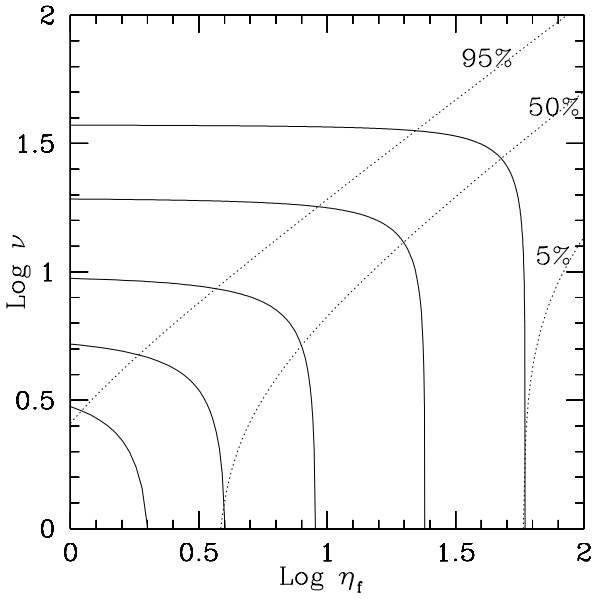

Fig. 7.— The evolution of column density η_f of the clump against the parameter ν. As soon as the clump is exposed to an FUV field, an outer column N_0 is instantaneously heated, and thus for ν marginally greater than 1, at $t = 0$, the final column density $\eta_f = \eta_{c0} - 1$. The figure shows how the final column density of the equilibrium clump configuration decreases with an increasing FUV field. Also shown are the contours depicting the percentage of mass lost from the clump as it photoevaporates.

Figure 7 shows a plot of the final column density of a clump, η_f, as it is exposed to various FUV fields, measured by ν, for $\alpha = 1$, $\beta = 1$ and $\gamma = 4/3$. The figure shows trajectories followed by the clump column density as the FUV field is increased, as might happen when the clump slowly emerges into the PDR region from the shielded interior of the molecular cloud. Note that the abscissa is η_f and not the initial column density η_{c0}. The outer column of cold clump gas N_0 that is initially heated is thereby discounted, and as soon as the FUV field is "turned-on" at time $t = 0$, $\eta_f = \eta_{c0} - 1$. As the FUV field (ν) increases, the clump begins to lose mass due to heating of the outer shell, and its column density begins to decrease with increasing ν. As ν approaches the critical value for complete photodissociation for that particular η_{c0}, the column density rapidly decreases with ν and the clump photoevaporates completely. If the final strength of the FUV field is less than that required for complete photoevaporation, the clump column density remains fixed at a point on its trajectory, as determined by the value of the parameter ν. Therefore, given a clump's initial column density and the strength of the local FUV field, the final column density of the clump can be determined. Equivalently, the observed η_f and ν can be used to determine the initial column η_{c0} of the clump. The total mass loss of the clump during its evolution can also be evaluated from equation (24). Figure 7 also shows the contours for the mass loss being 5%, 50% and 95% of the initial mass, for different values of η_f and ν.

The evolution of a clump with an isothermal density profile can be determined analogously. The initial density distribution in the clump is given by $n(r) = n_{cs0} r_{c0}^2 / r^2$, where n_{cs0} is the density at the clump surface, and the initial mass of the clump is $4\pi m_H n_{cs0} r_{c0}^3$. We assume that the density in the heated PDR shell in the final configuration of the clump is constant. Utilizing equations(21-23) for this case, we obtain an equation very analogous to equation (24) where now

$$\xi = \left(3\eta_{cs0}^3 - 3\eta_f^3 - \frac{3}{4}\eta_f^2 \right)^{1/2} - \frac{3}{2}\eta_f \tag{27}$$

$\eta_{cs0} = n_{cs0} r_{c0} / N_0$ and $\eta_f = n_{cs0} r_f / N_0$. An effective average column density through the clump can be defined by the ratio of the mass to area of the clump, $\bar{\eta}_{c0} = m_{c0} / (\pi r_{c0}^2 m_H N_0) = 4\eta_{cs0}$. The evolution of a clump with an isothermal density profile is thus qualitatively similar to that of a constant density clump, but with a different effective column density for the same mass. These solutions apply to clumps that are massive enough for gravity to be important in determining their density structure, and therefore have appreciable central density concentrations.

6. Numerical code and results

In the above analysis, simplifying approximations were made, which are now relaxed in a numerical code to obtain complete and more exact solutions (see Appendix D for details). One of the major differences between the numerical code and most of the analytic equations is the inclusion of gravity in the numerical code.

6.1. Impulsively heated clump in a vacuum

We first discuss the results of a numerical simulation of a clump generated by turbulence and heated impulsively. This case is hereafter referred to as Case V (for "vacuum"). A vacuum boundary condition is used so that the clump is free to expand, even in the absence of any heating. Initially, the thermal, turbulent and magnetic pressures in the clump are all assumed to be equal ($\alpha = \beta = 1$), and the magnetic pressure scales with the density to the power $\gamma = 4/3$. The FUV field is turned on instantly (t_{FUV}=0). The clump is assumed to be a constant density sphere, with a column density given by $\eta_{c0} = 10$, and in a FUV field characterized by $\nu = 10$ in the outer layers. The value of η_{c0} corresponds to that typical of clumps in clouds, for example, $m_c = 0.8 M_\odot, n_c = 2 \times 10^5 \mathrm{cm}^{-3}$, and $r_c = 0.03$pc. Clumps exposed to FUV fields with $G_0 \sim 10^5$ are heated to $T_{PDR} \sim 1000$K on their surfaces; if their shielded centres are $T_c \sim 10K$, then the ratio of sound speeds $\nu \sim 10$. These initial conditions imply the clump lies in the shock compression regime of Figure 2, and we expect from our analytic solutions that it should photoevaporate in less than one sound crossing timescale t_c (from eq. [11])

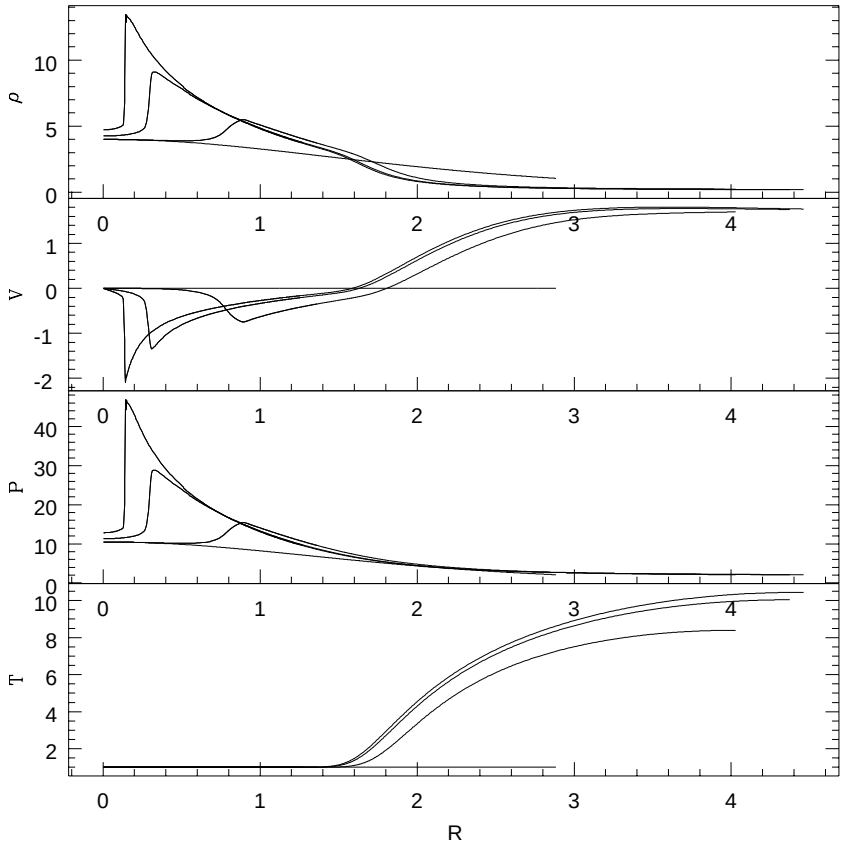

Fig. 8.— Density, velocity, pressure and temperature as a function of radius at times $t = 0.05, 0.1$, and $0.15 t_c$. The density, pressure and temperature are scaled to the initial values in the clump and the velocity is in units of the clump thermal speed c_c.

Figure 8 shows the density, velocity, pressure and temperature profiles in the gas as a function of radius at three different instants of time, $t = 0.05t_c, 0.1t_c$ and $0.15t_c$. As the outer layers heat up and the increased thermal pressure causes them to expand, a shock propagates into the clump, compressing the cold inner clump gas. The shock strengthens as it progresses to the centre of the cloud, as evidenced by the increasing density and velocity at the position of the shock front. The central cold gas gets compressed to very high densities, mainly due to the convergence of the radially-moving shocked gas. In Figure 8 we only show the evolution prior to the shock reaching the centre of the cloud. After the shock reaches the centre, the compressed gas rebounds and the cold inner clump undergoes radial oscillations as it settles into pressure equilibrium with the warm, expanding PDR outflow in the outer layers. The mean density of the compressed clump gas increases with time, as expected from our analytical solutions (eq. [B7]). As the clump loses mass, the FUV penetrates deeper and the clump is completely photoevaporated in $0.7t_c$. Our analytical solution (eq. [11]) predicts a photoevaporation timescale of $0.5t_c$, which agrees very well with the numerical solution. The photoevaporation timescale derived for a clump with this column density, $\eta_{c0} = 10$, and density, radius and sound speed given by $n_c = 2 \times 10^5 \mathrm{cm}^{-3}, r_c = 0.03\mathrm{pc}, \mathrm{and}\ c_c = 0.3\mathrm{kms}^{-1}$ respectively, is 10^4 years.

6.2. Gravitational collapse

The compression of a clump by strong shocks due to FUV heating can raise the central densities by large factors. This, however, did not render the clump gravitationally unstable to collapse in the above case because γ was chosen to be 4/3, which raises the magnetic pressure in dense gas sufficiently to prevent gravitational collapse (Chandrasekhar 1961). The scaling index of the magnetic pressure with density in clumps depends on the orientation of the magnetic field in the clump, and on whether the field is frozen into the neutral gas. For a frozen, uniform, unidirectional magnetic field, $P_B \propto n^{4/3}$. The magnetic field configuration in clumps is considerably more complicated (Ward-Thompson et al. 2000), and ambipolar diffusion may allow the neutral gas to slip past magnetic flux lines; making it difficult to define γ unambiguously.

We investigate the possibility of triggering gravitational collapse in clumps through a simulation where we adopt $\gamma = 1$, and all other parameters identical to those in Case V. Such a clump is expected to undergo gravitational collapse based on our earlier analysis (eq. [16] where $\eta_{c0} = 10$, and Figure 5).

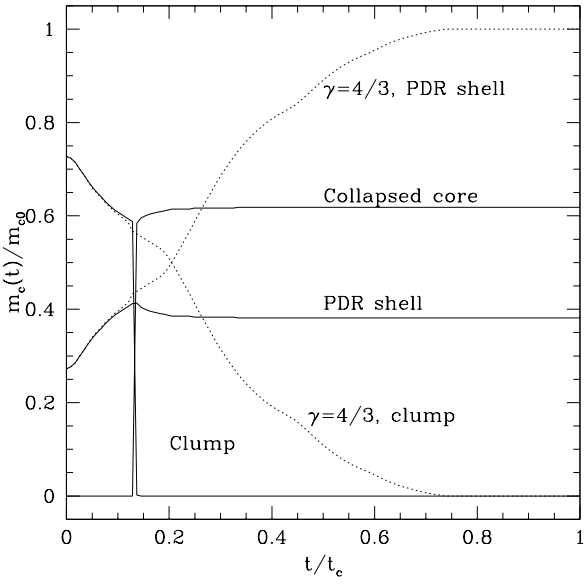

Fig. 9.— This figure shows the mass in the clump, core and warm PDR shell as a function of time. At collapse, the clump mass drops sharply to zero. Also shown in dotted lines are the clump and PDR shell masses for the case where $\gamma = 4/3$.

The evolution of the clump is initially similar to that in Case V. The outer surface expands, and a shock is driven into the clump centre. As the shock reaches the centre, the density of the cold clump gas increases and the clump radius decreases, until the central region becomes gravitationally unstable. A collapsing "core" is thus formed. This can be seen in Figure 9, which shows the mass of the clump as a function of time. The mass of the collapsing core is also shown in the figure, along with the results of Case V. The core mass is seen to increase above that contained in the clump just before collapse as the core accretes mass from the warm PDR gas. A significant fraction (60%) of the initial clump mass is driven gravitationally unstable to collapse, on very short timescales. In the absence of sufficient magnetic field support, exposure to strong FUV fields can thus trigger star formation in clumps. We also conducted a simulation with a weaker FUV field ($\nu = 5$), and found that the central regions collapsed in that case too, but the collapsing core contained only about 10% of the initial clump mass. Although these triggered collapse solutions are interesting and instructive, we emphasize that for initially stable clumps with $\beta \approx 1$, they hold only for $\gamma < 4/3$, which requires ambipolar diffusion. Since ambipolar diffusion timescales are longer than the shock compression timescale, it is likely that realistic clumps require $\gamma \geq 4/3$ and that triggered collapse does not often occur.

6.3. FUV heating of a pressure-confined clump: $t_{FUV} \gg t_c$

Pressure confined clumps are modelled as Bonnor-Ebert spheres which are in hydrostatic equilibrium. We construct a Bonnor-Ebert sphere by setting up a density distribution for a clump with thermal, magnetic and turbulent pressure support and in hydrostatic equilibrium. The density in the clump decreases as r^{-2} in the outer regions (similar to an isothermal sphere distribution), and flattens out in the central regions. The ratio of central to surface density x, determines the stability of the sphere against gravitational collapse, with a value exceeding 14.4 being "critically unstable" for an isothermal, non-magnetic gas. In these runs with a confining ICM, the outer 200 zones are used to represent the ICM. The ICM has the same pressure as the surface of the clump and is a constant density medium with a density (and temperature) contrast of 1000. As discussed in §4, for clumps confined by an ICM, a slow turn-on of the FUV field may be more appropriate. The FUV field in the numerical run is turned on in a time $t_{FUV} = 5t_c$, and we increase the temperature on this timescale so that the heated outer shell reaches its maximum temperature at $5t_c$.

Figure 10 shows the results for a case with varying x and where $\eta_{c0} = 10, \nu = 5, \gamma = 4/3$, and $\alpha = \beta = 1$. For Bonnor-Ebert spheres with $x \gtrsim 6$, the outer region with an isothermal density profile contains more than half the mass, and the clump evolution resembles that of

an isothermal sphere. In the figure, the mass of the clump is shown with time along with the analytical results for an isothermal sphere and a constant density sphere with the same initial column. The numerical results for three values of the central to surface density ratios, $x = 1, 3$ and 6 are indicated. For central concentrations greater than that represented by $x = 6$, the analytical results for an isothermal pressure-confined sphere match the numerical results, and the agreement increases as x increases and the Bonnor-Ebert clump configuration approaches a $1/r^2$ density profile. For $x = 1$, the clump is a constant density sphere, and the corresponding analytical calculations apply. A slight discrepancy can be noted in the figure between the two results, and this is due to the differences in the more realistic numerical model, i.e. an exponential drop in the PDR shell temperature with column and the inclusion of gravity. For intermediate central density concentrations, as represented by the case with $x = 3$, the mass loss rate is in between the two analytical extremes, as expected.

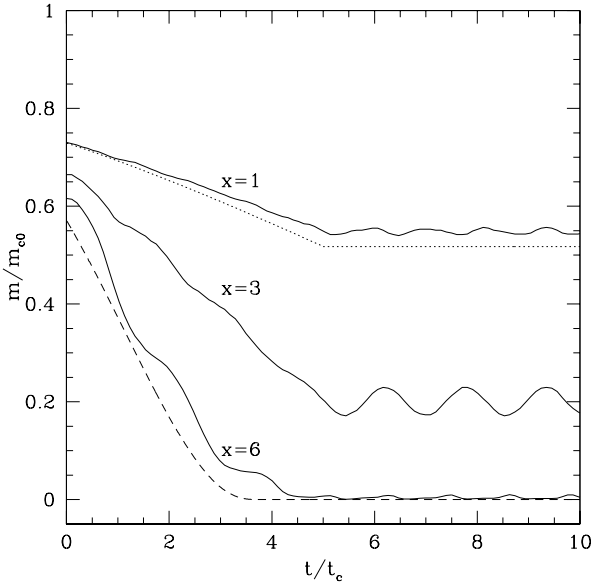

Fig. 10.— This figure shows the evolution of mass with time for a slowly heated, pressure-confined clump (Bonnor-Ebert sphere) with varying central to surface density ratios, $x = 1, 3$ and 6. In this case, $\eta_{c0} = 10, \nu = 5$, and $t_{FUV} = 5t_c$. The corresponding analytical solutions for a constant density sphere (dotted line) and an isothermal sphere (dashed line) are also shown for comparison.

7. Acceleration of clumps due to rocket effect

Spherically asymmetric mass flows from photoevaporating clumps can cause a rocket effect on the clump, as first noted by Oort & Spitzer (1955) in their theory on cloud acceleration by ionizing radiation from OB stars. Clumps exposed to FUV radiation in PDRs see a stronger incident flux of photons from the direction of the OB stars, though a significant flux due to backscattered radiation from dust on the opposite surface tends to reduce this asymmetry (see §5.2). The front and back hemispheres of the clump (with respect to the OB star) are thus heated to different temperatures (different ν) and the escaping material has a higher flow velocity on the star-facing surface of the clump. The net thrust on the clump accelerates it away from the star, and is known as the rocket effect. With the help of our analytical expressions for the evolution of an impulsively-heated, photoevaporating clump in a PDR, we now evaluate a simple criterion which determines the clump size at which the rocket effect becomes significant.

A simple 1-dimensional formulation for the acceleration due to the rocket effect is given by

$$\frac{dv_R}{dt} = -\frac{1}{m_c}\frac{dm_c}{dt}(v_{ff} - v_{fb}) \tag{28}$$

where v_{ff} and v_{fb} are the flow velocities at the front and back surfaces respectively and are assumed equal to the PDR sound speed c_{PDR} at those surfaces. We first compute the acceleration due to the flow from each hemisphere separately, take the difference to estimate the net acceleration, and then calculate the net velocity v_R attained by the clump. The mass loss from a hemisphere is given by $2\pi r_c(t)^2 \rho_b c_{PDR}$, where ρ_b is the density at the base of the flow. Taking only the component of the momentum in the flow along the direction to the star, we obtain

$$\left(\frac{dv_R}{dt}\right)_{1/2} = \frac{c_{PDR}}{m_c}\pi r_c(t)^2 \rho_b c_{PDR} \tag{29}$$

The net acceleration on the clump is therefore given by

$$\frac{dv_R}{dt} = \frac{\pi r_{fc}^2}{m_c}\left[(\rho_b c_{PDR}^2)_f - (\rho_b c_{PDR}^2)_b\right] \tag{30}$$

where the suffixes f and b denote the quantities for the front and back surfaces of the clump, and the clump radius r_{fc} is determined by the dominant flux on the front surface. As the initial expansion/compression phases in the evolution of a photoevaporating clump are typically short (see §5), we ignore this initial phase of evolution and assume the clump is evolving such that its column density is at its critical value $\eta_{crit} \sim 4\nu^2/3$, for the standard values of α, β and γ (see eq. [6]). Along with the relation for the column through the flow

$n_b(t)r_c(t) = 2N_0$ for each surface and the mass of the clump $m_c = 4\pi m_H n_{fc} r_{fc}^3/3$, (see appendix, eq. [A2]), we thus obtain for the net acceleration of the clump,

$$\frac{dv_R}{dt} = \frac{9}{8}\frac{c_c^2}{r_c}\left[1 - \frac{(c_{PDR}^2)_b}{(c_{PDR}^2)_f}\right] \tag{31}$$

The clump will remain in the PDR of the GMC and be subject to photoevaporation if the rocket velocity v_R attained in a time $t_{PDR} = X_{PDR}/v_{IF}$ is less than v_{IF}, or equivalently if

$$r_c > \frac{9}{8}\frac{c_c^2}{v_{IF}^2}\left[1 - \frac{(c_{PDR}^2)_b}{(c_{PDR}^2)_f}\right] X_{PDR} = r_R \tag{32}$$

There is thus a critical size r_R of clumps, where for $r_c < r_R$ they get rocketed back into the shielded molecular cloud, and for $r_c > r_R$ remain in the PDR and get photoevaporated or survive to photoevaporate in the H II region. For example, for front and back surface flow velocities of 3 km s^{-1} and 2 km s^{-1} respectively, $c_c = 0.3$ km s^{-1} and $v_{IF} = 0.5$ km s^{-1} equation (32) gives a critical clump size $r_R = 0.225X_{PDR}$. Clumps much smaller than this will get rocketed back into the molecular cloud as soon as they enter the PDR, partially evaporating in the process. We emphasize again that the rocket effect is significant only for turbulent clumps which undergo impulsive heating and photoevaporative flows. Pressure-confined clumps are gradually heated on their exteriors and do not go through phases of evolution with rapid mass outflows, and hence experience an insignificant rocket effect.

The mass lost by a clump before it gets accelerated out of the PDR can be estimated by integrating equation (28) with time, where only the components of velocity and mass flow along the direction towards the source are to be considered. Thus the mass of the clump is approximately given by

$$m_c(t) = m_{c0}\exp(-2v_{IF}/\Delta c_{PDR}) \tag{33}$$

where Δc_{PDR} is the difference in the flow velocities on the two sides of the clump. For typical values of $\Delta c_{PDR} = 1$ km s^{-1}, and $v_{IF} = 0.5$ km s^{-1}, in the time it takes for v_R to reach v_{IF}, the clump loses about 63% of its initial mass. Therefore clumps which are rocketed back into the cold molecular cloud interior also lose significant fractions of their mass before they attain high enough velocities to keep up with the advancing ionization front.

8. Discussion

We begin our discussion by summarizing our results for both the case where clumps are produced by turbulence in regions with insignificant interclump pressure and the case where clumps are initially stable structures confined by interclump pressure.

Consider first the scenario where clumps are continually generated by turbulence in the molecular clouds and the PDR. Initially, the evolution of the clump is determined by its column and the strength of the FUV flux. If $\lambda > 1$, or $\eta_{c0} > 4\nu^2/3$ for $\alpha = 1$, $\beta = 1$ and $\gamma = 4/3$, there is a very brief period of shock compression but the shock quickly dissipates before making it to the clump centre and the clump radius shrinks only slightly. Subsequently, the clump expands until $\lambda \approx 1$, at which point the photoevaporative flow halts the expansion and proceeds to shrink and compress the clump gas, maintaining $\lambda = 1$, or a column $n_c r_c = 4\nu^2 N_0/3$. If $\lambda < 1$, then the shock propagates to the centre of the clump, compressing it significantly, followed by an evolution at $\lambda \simeq 1$ identical to that above.

During the final $\lambda = 1$ evolution of the shrinking, compressing, evaporating clump, the rocket effect may play a significant role depending on the physical size of the clump at this time. If $r_c \lesssim r_R$, the clumps will be accelerated into the molecular cloud, losing a significant fraction of their mass in the process. If $r_R < r_c \lesssim X_{PDR} c_c / v_{IF}$, the clumps will tend to evaporate in the PDR region. However, because in the turbulent model clumps are forming in the PDR, including the region near the IF, some of these clumps will survive to enter an advancing H II region. If $r_c \gtrsim X_{PDR} c_c / v_{IF}$ and an H II region is advancing, then most of these large clumps will survive to be engulfed by the H II region.

The lifetimes of turbulent clumps are of order several sound crossing times of the initial size of the clump (Eq.[11] and Eq.[20]). As discussed previously, this is somewhat longer than clump lifetimes in the absence of an FUV field. Since turbulent clumps are being continuously formed, the steady-state abundance of clumps could actually increase in the presence of an FUV field.

Based on these results, the following predictions can be made for the turbulent scenario of photoevaporating clumps in PDRs.

1. There will be an enhanced population of clumps with columns $n_c r_c \approx 4\nu^2 N_0/3$. Note that this implies that in comparing this population from one PDR to another, the PDR with the lower ν (e.g., due to lower G_0) will have clumps with smaller column densities.

2. There will be a population of small clumps ($r_c \lesssim r_R$) moving with velocity $v \sim v_{IF}$ into the molecular cloud at $A_v \gtrsim 1$.

3. Compared with clumps in FUV-shielded regions, the clumps in turbulent PDRs will be smaller, denser and potentially more numerous.

4. Similarly, the clumps entering the H II regions will be smaller and denser than the molecular cloud clumps, and will have columns peaked at $4\nu^2 N_0/3$.

We note here that in the present analysis, turbulent clumps are geometrically idealized as constant density spheres. In reality, turbulently generated structures may also be sheet-like or filamentary in nature. Let us consider two simple representations of these geometries, disks and cylinders. For these structures to survive immediate photodissociation, the column density through their shortest dimension has to be greater than N_0. Disks with larger column densities through their midplane establish photoevaporative flows in an FUV radiation field. When the outer boundary of the heated gas reaches a distance equal to the radius of the disk, the flow diverges and the density in the flow (refer Eq.[A1] and Eq.[A2]) begins to drop as r^{-3} if $v \propto r$. Therefore, the mass loss rate from the disk is essentially similar to that of a spherical clump of size equal to the disk radius (Johnstone et al. 1998) Photoevaporative flows from a cylindrical structure differ slightly from those off a spherical clump of the same radius. The density at the base of the flow is now $\propto v^{-1}r^{-1} \propto r^{-2}$ and therefore, the critical column density $\eta_{crit} \approx 2\nu^3/3$. The mass loss rate from the cylindrical clump (following shock compression or initial expansion) no longer depends on the radius and is a constant given by $-2\pi m_H N_0 c_{PDR} l$ where l is the length of the cylindrical filament. (cf. Eq.[B11]). In summary, for turbulent clumps which are likely to be sheets or filaments, the mass loss from a thin sheet or disk of dimension r is best modelled as a clump of radius r. The mass loss rate from a disk of radius r and thickness t is similar to that of a sphere of radius r and is $\propto r$, but the evaporation timescale is $m/(dm/dt) \propto r^2 t/r \propto rt$ and hence much smaller than the sphere ($m/(dm/dt) \propto r^2$) for $t \ll r$. Filaments of radius r evolve somewhat differently than spheres of radius r; their mass loss rates do not decline as r shrinks. However, the evaporation timescales evolve similarly for cylinders or spheres since for spheres $m/(dm/dt) \propto r^3/r \propto r^2$, whereas for cylinders $m/(dm/dt) \propto r^2 l/r^0 l \propto r^2$.

Consider next the scenario where clumps are pressure-confined structures which are bounded by a low-density ICM, and the FUV turn-on timescale is of order the crossing time X_{PDR}/v_{IF} for clumps through the PDR. For small clumps with $r_c \lesssim X_{PDR}c_c/v_{IF}$, the FUV turn-on time $t_{FUV} > t_c$, which means that the FUV quasi-statically heats and expands an outer PDR surface on the clump, continually maintaining a pressure P_{ICM} in the PDR region and in the cold clump region. Again, the evolution of the clump is determined by its column and the strength of the FUV flux. If $\eta_{c0} < 0.48\nu^{4/3}$ (for $\alpha = 1, \beta = 1$, and $\gamma \geq 1$), the clump is completely heated and photodissociated as it enters the PDR from the molecular cloud. If $\eta_{c0} > 0.48\nu^{4/3}$, the clump shrinks to a smaller cold clump surrounded by a PDR shell. Since the evolution is quasi-static, there is insignificant rocket effect on these clumps. In this scenario, small cold clumps, protected by PDR shells, can survive passage through the PDR and into the H II region. However, the minimum initial column for such a clump is $\eta_{c0} \approx 0.48\nu^{4/3}$ (for $\alpha = 1, \beta = 1$, and $\gamma \geq 1$).

For large clumps, $r_c \gtrsim X_{PDR}c_c/v_{IF}$, $t_{FUV} < t_c$, which means that shocks compress

the clump and strong photoevaporative outflows are initiated as the clump enters the PDR. Clumps with $1 < \eta_{c0} < 4\nu^2/3$, are compressed by shocks which propagate to the centre, but they finally relax to an analogous situation as above, i.e., a thick PDR shell surrounding a small mass cold clump if $\eta_{c0} > 0.48\nu^{4/3}$ and totally photodissociated otherwise. Clumps with $\eta_{c0} > 4\nu^2/3$ have a brief period of shock compression and PDR expansion, but rapidly relax to a configuration with a thin PDR shell and most of the initial mass still in the cold shielded core. All the large clumps experience a rocket effect. However, as shown earlier, large clumps with $r_c > r_R$ do not experience enough rocket acceleration to prevent them from entering the H II region. Therefore, in the ICM confined scenario, a variety of clump sizes enter the H II region. However, the small clumps entering the H II region were initially clumps of larger size and mass in the molecular cloud, and they enter the H II region with large protective PDR shells.

One can compare the abundance of clumps of various sizes in PDRs with the abundance of clumps in the molecular cloud, under the assumption that ICM-confined clumps are long-lived (the formation time of clumps exceeds the crossing time X_{PDR}/v_{IF}). Small cold clumps are converted to PDRs but larger cold clumps are converted to small cold clumps with PDR shells and this partially replaces the small clump population. Thus, there will be a significant drop in the cold clump population with $\eta_{c0} < 4\nu^2/3$. However, the population $\eta_{c0} > 4\nu^2/3$ is little affected. Therefore, a variety of clump sizes enter the H II region, but there is a suppression of clumps with columns $\eta_{c0} < 4\nu^2/3$ compared to the distribution in the shielded molecular cloud.

Based on these results, the following predictions can be made for clumps initially confined by interclump pressure.

1. Compared with small cold clumps ($\eta_{c0} < 4\nu^2/3$) in similar pressure regions of the molecular cloud, clumps of the same column density in PDRs will have a smaller relative population. Correspondingly, small and large clumps enter the advancing H II regions, but the relative number of small clumps is suppressed.

2. Larger clumps are relatively unaffected, but do experience an initial transient period of shock compression and photoevaporative flow.

3. Small clumps ($\eta_{c0} < 4\nu^2/3$) in the FUV-illuminated region will have small masses relative to their PDR shells.

We have shown that small clumps tend to be destroyed before they are overtaken by the ionization front of the advancing H II region. This would affect the number, size distribution,

and structure of pressure-confined clumps that enter an H II region, and therefore affect the evolution of the H II region (see Bertoldi 1989 and Bertoldi & McKee 1990 for a discussion of the effect of photoevaporating clumps on the evolution of an H II region). Clumps that survive to enter the H II region will thus have undergone significant evolution from their initial states. These clumps could be considerably denser if they are still vigorously photoevaporating as they enter the H II region, where they continue to photoevaporate (Bertoldi 1989, Bertoldi & McKee 1990). We will discuss the propagation of clumps into H II regions in a separate paper, with application to the Eagle Nebula.

We conclude our discussion by using our results to critique the previous inferences of dense ($\sim 10^7$ cm^{-3}) FUV heated clumps in PDRs and to propose several observational consequences of our results.

Our photoevaporation models provide arguments against the interpretation that dense ($n \sim 10^{6-7}$ cm^{-3}) PDR surfaces of clumps give rise to the observed high excitation CO lines. The fundamental problem is the propagation of the FUV photons to regions of such high density. If densities of $\sim 10^{6-7}$ cm^{-3} are in fact heated to $T \gg 100$K, then the thermal pressures in these regions are much larger than the pressures in the interclump gas. The only way this is possible is if: (i) the clumps are gravitationally bound or (ii) the warm surface regions are photoevaporating, as discussed in this paper. In either case, the density in the clump will smoothly fall off with radius, $n(r) \propto r^{-b}$ where $b \sim 2-3$, until the transition to the ICM. However, FUV photons which heat the CO are only able to penetrate through a column $N_0 \sim 2 \times 10^{21}$ cm^{-2}, where

$$N_0 \approx \int_r^\infty n(r)dr \approx \frac{1}{b-1} n(r) r \tag{34}$$

This equation reveals the size r of the FUV heated region if a density $n(r)$ is required in this region. It implies that for the FUV to heat gas at densities $\gtrsim 10^6$ cm^{-3}, the clumps must be very small with size scales of $r \approx N_0/10^6$ cm^{-3} $\approx 2 \times 10^{15}$ cm at this density. Gravitationally bound clumps have densities $n \sim 10^{6-7}$ cm^{-3} at sizes $\gg 10^{15}$ cm (e.g., Shu 1977). In such clumps, the FUV would not penetrate to such high densities, but would be absorbed in the lower density regions further out. Such small scales as 10^{15} cm also argue against unbound clumps explaining the high temperature CO emission. We have shown in this paper that such a small clump will either be rocketed out of the PDR or photoevaporate in roughly a sound crossing time, or ~ 300 years, a time so short as to rule out this possibility.

The size scale of 100 AU is suggestive of disks around young stars rather than clumps, so that one might appeal to photoevaporating disks like the "proplyds" in Orion (e.g., Johnstone et al. 1998). Here, the enormous mass reservoir of the disk greatly lengthens the photoevaporative timescale. However, the area filling factor of these photoevaporating disks

required to match the CO high-J line intensities in, for example, the Orion Bar region is of order ~ 0.1 (Burton et al. 1990). Such a high area filling factor requires a volume density of $\gtrsim 3 \times 10^5$ stars pc^{-3}, more than an order of magnitude higher than that observed in the densest region of the stellar cluster near the Trapezium (McCaughrean et al. 1994). Photoevaporating proplyds are thereby also ruled out.

Therefore, it seems quite unlikely that FUV radiation is heating dense, $n \sim 10^{6-7}$ cm^{-3}, PDR surfaces of clumps or that photoevaporating proplyds can explain the mid-J CO emission. We suspect that the CO emission arises in $n \sim 10^5$ cm^{-3} surfaces of large ($\gtrsim 10^{16}$ cm) clumps, and that the chemistry, heating and/or dynamics needs to be modified in PDR models in order to better match the observations.

There are several observational consequences implicit in the scenario of a strongly photoevaporating (i.e., $t_{FUV}/t_c < 1$) clump. First, the molecular material from the clump core is effectively advected out into the PDR region, as has been discussed by Bertoldi & Draine (1996), Störzer & Hollenbach (1998), Hollenbach & Tielens (1999). This can have strong effects on the chemistry, primarily because H_2 can exist in surface regions where it would have been atomic in a stationary, steady-state case. In turn, the higher abundance of H_2 can chemically enhance the abundance of other minor species, such as H_3^+ (Bertoldi & Draine 1996) and CO and can modify the heating and cooling processes and therefore the PDR temperature. Initial results (Störzer & Hollenbach 1998 and Störzer 2000, private communication) suggest that advection will enhance the intensities of the mid-J CO lines, by creating more warm CO near the surface. Finally, the flow will broaden line widths to values $\Delta v_{FWHM} \sim c_{PDR}$. However, it should be noted that many common molecules, such as CO, HCO^+, CS, HCN, CN still exist primarily at column depths $N > N_0$ from the surface, where the advection velocities are low. Broader linewidths should be seen in C II(158μm),O I(63μm) and possibly the H_2 (2μm) lines.

9. Applications to observed PDRs in well-studied star forming regions

We compare our results with available observational data on clump characteristics from some well-studied star-forming regions, the Orion Bar, M17SW, NGC 2023 and the PDR surrounding the Rosette Nebula. Clump column densities (η) can be estimated from measured or inferred densities and sizes of clumps in these PDRs. Densities are usually inferred indirectly from comparing observed line intensities and line ratios with available PDR chemical models in most of these cases. Clump sizes are ill-determined, as they are usually too small to be resolved directly and only upper limits to the sizes are available, with the PDRs in Rosette and NGC 2023 being possible exceptions. The FUV field strengths in these PDRs

can be estimated more accurately, as the luminosities of the illuminating O/B stars is reasonably well-determined. We use these field strengths and the dust temperature models of Hollenbach, Takahashi & Tielens (1991) to estimate the temperature of dust in the shielded clump interior. As the interior gas temperature is closely coupled to the dust temperature, we set the two equal and thus determine the sound speed c_c in the cold clump gas. The temperature to which the FUV field heats the surface clump gas is determined from the PDR models of Kaufman et al. (1999), and thus c_{PDR} is obtained, allowing us to estimate the value of the parameter ν in each region. Below we first determine η and ν for each observed region, and then use these parameters, compared to Figures 2 and 7, to infer their nature and evolution.

Orion Bar The Orion Bar has been observed in many atomic and molecular line transitions in the sub-millimeter and infrared wavelength regions (e.g. van der Werf et al. 1996, Tauber et al. 1994, Young Owl et al. 2000, Marconi et al. 1998). The molecular line emission peaks at about 0.03 pc from the IF, and the gas between this dense ridge and the IF is mainly neutral atomic hydrogen. The observed line intensities and line ratios appear to be best explained by a two-component model for the PDR gas, with small ($\lesssim 0.02$ pc) dense ($n_c \sim 10^{6-7}$ cm^{-3}) clumps, required to match the line emission and an interclump medium $n_{ICM} \sim 10^{4-5}$ cm^{-3} which causes the chemical stratification of the edge-on PDR. The local FUV field is estimated as $G_0 \sim 4 \times 10^4$. Such an FUV field incident on clumps with these inferred densities would heat their surfaces to temperatures $\sim 2000-5000$ K (Kaufman et al. 1999). The gas temperature in the interior of clumps exposed to this FUV flux is expected to be ~ 50 K (Hollenbach et al. 1991). We thus obtain $\eta \sim 15 - 150$ and $\nu \sim 8 - 10$.

M17 SW Multilevel molecular line observations in CS (Wang et al. 1993, Evans et al. 1987) and in several fine structure lines (C II, Si II, O I, Meixner et al. 1992) indicate that the M17 SW cloud core consists of numerous high density clumps with densities $n_c \sim 1-5\times10^5$ cm^{-3}. Maps of CO^+ emission compared with theoretical models suggest that the emission is produced in the warm surface layers of PDRs in dense clumps (Störzer et al. 1995) of sizes $r_c \sim 0.1$ pc. The local FUV field near the H II region/molecular cloud interface is $G_0 \sim 8 \times 10^4$, which implies PDR temperatures of about 2000K on the clump surfaces and cold clump gas temperatures ~ 60K, therefore, $\nu \sim 4 - 9$. The column densities of clumps are typically $\eta = 7 - 35$, as estimated from typical densities and sizes (Meixner et al. 1992, Störzer et al. 1995).

NGC 2023 The well-studied PDR in the reflection nebula NGC 2023, at a distance of 475 pc, is illuminated by a B star and is well-studied (e.g., Wyrowski et al. 2000, Steiman-Cameron et al. 1997, Howe et al. 1991). Observations of atomic fine structure lines indicate the presence of clumpy gas in the PDR with densities $\sim 10^5$ cm^{-3}, and an ICM density of $\sim 10^3$ cm^{-3} (Steiman- Cameron et al. 1997). The PDR is situated about 0.1-0.2 pc away from the exciting star, and has a width $X_{PDR} = 0.04$ pc. The clumps have sizes ~ 0.05 pc (Wyrowski et al. 2000), and therefore $\eta_{c0} \sim 5$. The FUV field strength has been estimated at $G_0 = 10^4$, and from the PDR models of Kaufman et al. (1999), $c_{PDR} = 3$km s^{-3}. With a clump gas temperature of ~ 20 K for this value of G_0, we obtain $\nu = 5$. It should be noted that the level of turbulent energy in the NGC 2023 PDR as estimated from observed linewidths is low (Wyrowski et al. 2000), which suggests that clumps are not rapidly re-formed by turbulence in the PDR.

Rosette PDR The Rosette Nebula surrounding the young open cluster NGC 2244, is an expanding H II region at a distance of 1.6 kpc. The H II region/molecular cloud interface shows a distinct ridge of emission, with substructure on small scales down to 0.5 pc (Schneider et al. 1998). The PDR region is very extended, and the FUV photons penetrate deep into the cloud with an interclump medium density $n_{ICM} \sim 10$ cm^{-3} (Blitz 1991, Williams et al. 1995). The ICM near the edge of the HII region may even by partially ionized gas as suggested by the pervasive Hα emission observed (Block et al. 1992). This region has a low FUV field, with $G_0 \sim 200$ about 15 pc away from the OB star cluster, and dropping to lower values of 10-50, about 30 pc away from the cluster (Schneider et al. 1998). Clump densities required to match observed CII line intensities are $\sim 10^{4-5}$ cm^{-3}. Cold clump gas temperatures are calculated to range from $10-15$ K. The Rosette PDR thus has $\eta_{c0} \sim 5-35$ and $\nu \sim 5$, while further away from the H II region, $\nu \sim 2-3$.

Using the above determined values of the parameters η and ν for clumps in the above PDRs, we can locate them on the parameter plots of Figures 2 and 7. Figure 11 shows an overlay of our model results with inferred data for both the turbulent and pressure-confined clump models. The data are consistent with both clump models and, within the limits of the uncertainties in arriving at "observed" η and ν, agree reasonably well with our predictions. Turbulent clumps are expected to have columns fairly close to the critical value η_{crit} which is $\approx 4\nu^2/3$. The observed data lie near the $\eta = \eta_{crit}$ line, indicating that the observed clumps may be turbulent in origin and undergoing photoevaporation in the FUV field. The exception is NGC 2023. The clumps in this PDR are observed to have negligible turbulence, and are thus not expected to have a column equal to η_{crit}. The data are also consistent with clumps being pressure-confined. In such a situation, we would not expect to see clumps

beyond the 95% mass loss line, as seen in the figure. However, there does appear to be a weak trend of increasing η with ν, which if real is not easily explained in this model. The clumps in NGC 2023 are probably pressure-confined, and seem to have lost almost 75% of their original mass through FUV heating. High resolution observations of clumps in PDRs, with more accurate determinations of the sizes and densities of clumps would help in locating them more precisely on the $\eta - \nu$ plots, and thus be able to distinguish between the pressure-confined and turbulent clump models.

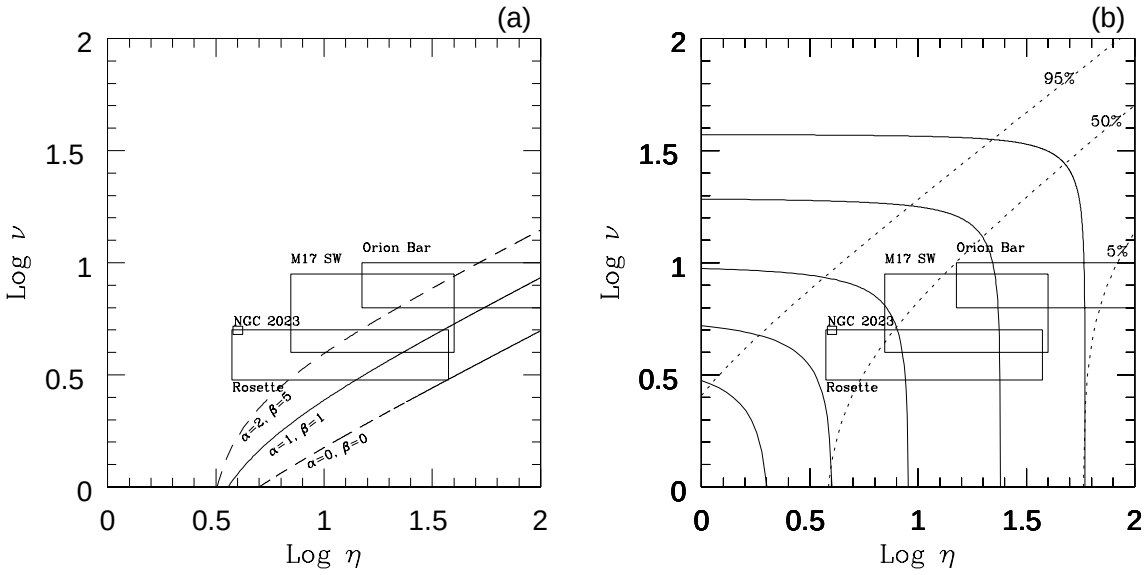

Fig. 11.— Observational data for some PDRs on the $\eta - \nu$ parameter plot for the turbulent (panel a) and pressure-confined (panel b) clump models. There is a slight indication that the columns lie along the $\nu^{4/3}$ lines expected in the turbulent model of clumps, with the exception of NGC 2023.

10. Conclusion

We have studied the effects of FUV radiation from young OB stars on the evolution of dense structures or clumps in photodissociation regions. We find that the ambient FUV field penetrates through the surface of a dense clump and heats this surface layer to high temperatures, causing mass loss and thereby inducing photoevaporation of the clump. Through analytic approximations and numerical hydrodynamical calculations, we determined the evolution and lifetimes of clumps, subject to various physical conditions and initial parameters.

The evolution of a clump is mainly determined by three parameters, the ratio of the initial column density to the column penetrated by the FUV flux, η_{c0}; the strength of the FUV field, which we denote by the ratio of the sound speeds in the heated gas and the cold clump material, ν; and the timescale for the turn-on of the FUV field, relative to the sound crossing time through the clump, t_{FUV}/t_c. We consider the evolution of turbulent, impulsively-heated clumps and also pressure-confined clumps in a PDR. Impulsively heated clumps with a photoevaporation parameter $\lambda \approx 3\eta_{c0}/(4\nu^2) < 1$ are initially compressed by a shock driven by the external high-pressure FUV-heated layer to high densities, and later lose mass as the FUV gradually penetrates through the entire clump. Clumps with $\lambda > 1$ go through an initial expansion phase after the rapid decay of the shock wave. Both clumps with $\lambda < 1$ and $\lambda > 1$ evolve toward the $\lambda = 1$ condition. The final evolution toward complete photodissociation and heating occurs at constant column through the clump, the density increasing as the clump shrinks. Photoevaporation timescales in all these cases are typically a few t_c, suggesting clump destruction times of $\sim 10^{4-5}$ years, under typical PDR conditions. Slowly heated clumps evolve quasi-statically, and if confined by an external ICM pressure, a fraction of the initial cold clump mass may be retained if $\eta_{c0} > 0.48\nu^2$. Clumps with initial column densities $\eta_{c0} < 0.48\nu^2$ are completely photoevaporated by the FUV flux.

We predict that in the turbulent scenario, observed clumps should all have columns close to the critical value for the local FUV field, $\eta_{crit} \approx 4\nu^2/3$. Clumps lifetimes are prolonged by photoevaporation and we also expect a higher steady-state abundance of clumps in PDRs as compared to the shielded molecular cloud interior. For pressure-confined clumps, there will be a decrease in the number of smaller clumps in PDRs, and many clumps will lose substantial fractions of their mass to extended warm PDR shells around them. We compared our results to observations of some well-studied PDRs, such as the Orion Bar, M17SW, NGC 2023 and the Rosette PDR, and find that the data are consistent with both clump models, but perhaps favour the turbulent clump interpretation. Clumps entering the H II region around an O/B star with a D-type ionization front are expected to have thus undergone significant evolution as they pass through the PDR.

We acknowledge support from the NASA Astrophysical Theory Program under RTOP 344-04-10-02, which supports the Center for Star Formation Studies. U. Gorti was supported by a National Research Council Associateship. We thank K. R. Bell, M. Kaufman, C. McKee and H. Störzer for useful discussions.

A. Analytic model: Unconfined clumps with $t_{FUV}/t_c \ll 1$

We first define several characteristic timescales during evolution. The initial sound crossing time through the clump is denoted by $t_c = r_{c0}/c_c$. We can similarly define a sound crossing time through the warm PDR layer, as $t_p = \delta_0/c_{PDR}$. Finally, we define the timescale for the PDR layer to expand to a thickness comparable to r_{c0}, $t_{e0} = r_{c0}/c_{PDR}$.

We relate the density n_b at the base of the PDR shell ($r = r_c$) to N_0 for epochs when the PDR shell has expanded to a thickness greater than the clump radius ($t > t_{e0}$). The FUV-heated shell of initial thickness δ_0 expands as an isothermal flow into vacuum and the characteristics of the flow regions are essentially similar to that of the Parker wind solution with no gravity (Parker 1958). For simplicity, it is assumed here that once the warm PDR region has expanded to $\delta \gtrsim r_c$ or $t > t_{e0}$, the gas leaves the clump surface at c_{PDR} and the velocity of the heated gas increases linearly with radius. Based on our hydrodynamical code results, this is a reasonable approximation to within about two clump radii, where most of the column density in the PDR gas lies. The clump mass loss rate is determined by the penetration depth of the FUV flux, and hence N_0. For a power law density profile in the shell ($n(r) \propto r^{-b}, b \gtrsim 2$), most of this column arises from the base of the shell, or, more precisely, from the region between the base (clump surface) r_c and $\sim 2r_c$. From the equation of continuity and $v \propto r$, the steady flow density profile of the warm PDR shell is obtained as,

$$n(r) \propto v^{-1} r^{-2} \propto r^{-3}, \tag{A1}$$

valid for $r_c < r < 2r_c$ once the shell has expanded to at least two clump radii ($t > t_{e0}$). Equation (A1) can be easily integrated over r to obtain the column through the warm PDR at any given instant of time. Let r_c denote the instantaneous cold clump radius and r_t the total radius of cold clump and warm PDR gas. At $t = 0$, $r_c = r_c(0) = r_{c0} - \delta_0$. Using the fact that $r_t \gg r_c$ for $t > t_{e0}$, and as the FUV flux always penetrates through a column N_0, we have

$$N_0 = \int_{r_c}^{r_t} n(r,t) dr \approx \frac{1}{2} n_b(t) r_c(t) \text{ for } t > t_{e0} \tag{A2}$$

We next write down the equations of momentum flux or pressure. The pressure in the shocked cold clump gas is the sum of thermal, turbulent and magnetic pressures and given

by

$$P_c(t) = n_c(t)c_c^2 + \alpha n_c(t)c_c^2 + \beta n_{c0}c_c^2(n_c(t)/n_{c0})^\gamma \tag{A3}$$

where $n_c(t)$ is the shocked clump density at time t, n_{c0} is the initial clump density, α is the initial ratio of turbulent and thermal pressures, and β is the initial ratio of magnetic to thermal pressure in the clump. The pressure at the base of the PDR flow, P_b, is given by

$$P_b(t) = n_b(t)(c_{PDR}^2 + \alpha c_c^2) + \beta n_{c0}c_c^2\left(\frac{n_b(t)}{n_{c0}}\right)^\gamma + n_b(t)v_{flow}^2, \tag{A4}$$

where v_{flow} is the outward flow at the base. We assume that $v_{flow} = c_{PDR}$, and from equations (A2) and (A4),

$$P_b(t) = 2\frac{N_0}{r_c(t)}(2c_{PDR}^2 + \alpha c_c^2) + \beta n_{c0}c_c^2\left(\frac{2N_0}{n_{c0}r_c(t)}\right)^\gamma \tag{A5}$$

The boundary between the "shock compression" and "initial expansion" regions of Figure 2 is determined by comparing equations (A3) and (A5). Values of the parameters η_{c0} and ν on this boundary are such that the shock dies out just before making it to the centre. The pressure in the clump at this instant is about the same as the initial pressure and $r_c(t_{e0}) \simeq r_c(0)$. In a time $t = t_{e0}$, the outer edge of the PDR shell expands out to $2r_{c0}$, and the initial PDR column begins to decrease appreciably due to spherical divergence, allowing further FUV flux penetration.

If $P_b(t_{e0}) > P_c(t = 0)$, the pressure in the PDR flow is sufficiently high for the shock wave to reach the centre of the clump, compressing the clump and raising its central pressure so that $P_b(t_{e0}) = P_c(t_{e0})$. Such clumps lie in the "shock compression" of Figure 2. If the initial parameters are such that $P_b(t_{e0}) < P_c(t = 0)$, the shock wave rapidly dies out before reaching the centre and the clump then stops contracting and begins to expand at a speed $\approx c_c$, maintaining pressure equilibrium. These two evolutionary sequences are separated by the (η_{c0}, ν) boundary obtained setting $P_b(t_{e0}) = P_c(t = 0)$, or from equations (A3) and (A5),

$$\frac{2(2\nu^2 + \alpha)}{\eta_{c0} - 1} + \beta\left(\frac{2}{\eta_{c0} - 1}\right)^\gamma = 1 + \alpha + \beta. \tag{A6}$$

For values of η_{c0} and ν typical in PDRs such as Orion ($\eta_{c0} \gg 1, \nu^2 \gg 1, \alpha = \beta = 1, \gamma = 4/3$) this relation can be approximated as $\eta_{c0} \approx 4\nu^2/3$. A photoevaporation parameter $\lambda = 3(\eta_{c0} - 1)/2(2\nu^2 + 1)$ can be defined such that the relation $\lambda = 1$ demarcates the two regions. Clumps with $\lambda < 1$ are shock compressed and those with $\lambda > 1$ initially expand.

B. Evolution of shock-compressed clumps

As the flow expands in a shock compressed clump, the clump shrinks by losing mass at a rate

$$\frac{dm_c}{dt} = -4\pi m_H n_b(t) r_c(t)^2 c_{PDR} \tag{B1}$$

Initially, a shock is driven into the clump, but we do not attempt to analytically model the propagation of the shock wave in detail. We assume that the shock travels inward at the PDR sound speed and the entire clump gets compressed in a time $t_s = r_c(0)/c_{PDR}$, where $r_c(0) = r_{c0} - \delta_0$. We first solve for the clump radius, mass and mass loss rate for $t < t_s$, during the epoch when the shock propagates to the centre.

We assume that the clump radius decreases with a constant speed $v_b (\lesssim c_{PDR})$ so that

$$r_c(t) = r_c(0) - v_b t. \tag{B2}$$

The mass of the cold clump decreases with time, and at t_s is given by

$$m_c(t_s) = m_c(0) + \int_0^{t_s} (dm_c/dt) dt \tag{B3}$$

where $m_c(0) = \frac{4}{3}\pi m_H n_{c0} {r_c}^3(0)$. From equations (A2), (B1), (B2) and (B3), we have

$$m_c(t_s) = m_c(0) - 8\pi m_H N_0 r_c(0)^2 (1 - v_b/(2c_{PDR})) \tag{B4}$$

We solve for v_b and thereby calculate $r_c(t_s)$. To do this we need to calculate the clump compression at t_s. The clump gets compressed by the shock to a new density $n(t_s)$ which can be determined from the condition of pressure equilibrium at the clump surface. The momentum flux conservation equation across the "front" which marks the boundary between clump and FUV heated flow is then

$$(1+\alpha) n_c(t_s) c_c^2 + \beta n_{c0} c_c^2 (n_c(t_s)/n_{c0})^\gamma = 2 n_b(t_s) c_{PDR}^2 + \alpha n_b(t_s) c_c^2 + \beta n_{c0} c_c^2 (n_b(t_s)/n_{c0})^\gamma \tag{B5}$$

In moderate to strong FUV fields, the PDR sound speeds and hence the shock velocities (assumed equal to c_{PDR}) are high, and the resulting compression is also high. As the magnetic pressure P_B, scales with a higher power of the density than the thermal pressure P_T, (we use $\gamma \gtrsim 4/3$) and as the initial magnetic pressure is comparable to the thermal pressure, the thermal contribution to the pressure in the compressed gas can be ignored. In the expanded flow, the density is low and here the thermal pressure and dynamical pressure dominate. Equation (B5) can be simplified to give the density of the compressed gas

$$\frac{n_c(t_s)}{n_{c0}} = \left(\frac{(2\nu^2 + \alpha)}{\beta} \frac{n_b(t_s)}{n_{c0}} \right)^{1/\gamma}. \tag{B6}$$

From equations (A2) and (B6),

$$\frac{n_c(t_s)}{n_{c0}} = \left(\frac{2\delta_0(2\nu^2+\alpha)}{\beta}\right)^{1/\gamma} r_c(t_s)^{-1/\gamma}. \tag{B7}$$

The mass of the clump at time t_s can also be expressed as

$$m_c(t_s) = \frac{4\pi}{3} m_H n_c(t_s) r_c(t_s)^3. \tag{B8}$$

From equations (B2), (B7) and (B8)

$$m_c(t_s) = \frac{4\pi}{3} m_H n_{c0} \left(\frac{2\delta_0(2\nu^2+\alpha)}{\beta}\right)^{1/\gamma} r_c(0)^{3-1/\gamma} \left(1 - \frac{v_b}{c_{PDR}}\right)^{3-1/\gamma}. \tag{B9}$$

At time t_s, the radius of the shock-compressed clump is $r_s = r_c(t_s) = r_c(0)(1 - v_b/c_{PDR})$ from equation (B2). The unknown parameter v_b is finally determined from equating the two expressions for the clump mass, equations (B4) and (B9). The evolution of the clump radius is thus known as a function of time for $0 < t \leq t_s$, from equations (B2),(B7) and the solution for v_b. These general equations are, however, fairly complex, and an approximate solution can be obtained for the case $\alpha = 1, \beta = 1$, and $\gamma = 4/3$ as,

$$r_s \approx q r_c(0) \left(1 - \frac{3(1+q)}{\eta_{c0} - 1}\right)^{4/9} \tag{B10}$$

where $q = (\lambda/3)^{1/3}$.

We now solve for the evolution of the clump for $t > t_s$. After being compressed by the shock, the clump continues to lose mass through photoevaporation, with a mass loss rate,

$$\frac{dm_c}{dt} = -4\pi m_H n_b(t) r_c(t)^2 c_{PDR} = -8\pi m_H N_0 r_c(t) c_{PDR} \tag{B11}$$

The mass of the clump at any given time ($t > t_s$) can also be written as

$$m_c(t) = m_c(0) \left(\frac{2(2\nu^2+\alpha)}{\beta(\eta_{c0}-1)}\right)^{1/\gamma} \left(\frac{r_c(t)}{r_c(0)}\right)^{3-1/\gamma}. \tag{B12}$$

From equation (B11) and differentiating equation (B12) with time, the radius of the clump as a function of time is given

$$r_c(t) = \left(\left(\frac{r_s)}{r_c(0)}\right)^{2-1/\gamma} - \frac{(2\gamma-1)}{(3\gamma-1)} \frac{6\nu\eta_{c0}}{(\eta_{c0}-1)^2} \left(\frac{\beta(\eta_{c0}-1)}{2(2\nu^2+\alpha)}\right)^{1/\gamma} \left(\frac{t}{t_c} - \frac{(\eta_{c0}-1)}{\eta_{c0}\nu}\right)\right)^{\frac{\gamma}{2\gamma-1}}. \tag{B13}$$

A photoevaporation timescale t_{PE} for the clump can be defined as the time for the radius of the clump to shrink to zero, and from equation (B13)

$$t_{PE} = t_c \left(\left(\frac{r_s}{r_c(0)} \right)^{2-1/\gamma} \left(\frac{3\gamma - 1}{2\gamma - 1} \right) \frac{(\eta_{c0} - 1)^2}{6\nu\eta_{c0}} \left(\frac{2(2\nu^2 + \alpha)}{\beta(\eta_{c0} - 1)} \right)^{1/\gamma} + \frac{\eta_{c0} - 1}{\eta_{c0}\nu} \right). \tag{B14}$$

For $\alpha = 1, \beta = 1$, and $\gamma = 4/3$, the above equations determining the evolution of the clump can be simplified as

$$r_c(t) = \left(\left(\frac{r_s}{r_c(0)} \right)^{5/4} - \frac{10\eta_{c0}\nu}{3(\eta_{c0} - 1)^2} q^{9/4} \left(\frac{t}{t_c} - \frac{(\eta_{c0} - 1)}{\eta_{c0}\nu} \right) \right)^{4/5} r_c(0), \tag{B15}$$

$$m_c(t) = m_c(0) \left(\frac{r_c(t)}{q r_c(0)} \right)^{9/4}, \tag{B16}$$

and

$$t_{PE} = t_c \left(\frac{3(\eta_{c0} - 1)^2}{10 q \eta_{c0}\nu} \left(1 - \frac{3(1+q)}{\eta_{c0} - 1} \right)^{5/9} + \frac{(\eta_{c0} - 1)}{\eta_{c0}\nu} \right). \tag{B17}$$

C. Evolution of clumps that undergo an initial expansion

Clumps with large initial column densities and in low FUV fields quickly evolve to the point where their internal pressures are greater than that of the (expanded) thin heated surface layer. They expand out into vacuum (as they would even in the absence of an external FUV field) at their sound speed c_c for a time t_e, until the pressure drops to that in the heated outer layer. At $t = t_e$, there is pressure equilibrium and equation (B5) again holds. The clump expands to a new radius $r_c(t_e) = r_c(0) + c_c t_e$ and during expansion loses mass at a rate given by equation (B1). The mass of the clump at $t = t_e$ is obtained as earlier,

$$m_c(t_e) = m_c(0) - 8\pi m_H N_0 c_{PDR} (r_c(0) t_e + c_c t_e^2/2). \tag{C1}$$

Also,

$$m_c(t_e) = \frac{4\pi}{3} m_H n_c(t_e) {r_c}^3(t_e)^3. \tag{C2}$$

Because there is significant expansion, $n_c(t_e) \ll n_{c0}$, we assume that thermal pressure dominates in both the clump and the PDR flow. From equations (B5) and (C2)

$$m_c(t_e) = \frac{8\pi}{3} m_H N_0 \frac{2\nu^2 + \alpha}{1 + \alpha} r_c(t_e)^2 \tag{C3}$$

Equations (C1) and (C3) can be solved for t_e, and

$$t_e = t_c \left(1 - \frac{1}{\eta_{c0}}\right) \left(\left(\frac{3\nu + \eta_{c0} - 1}{3\nu + 2(2\nu^2 + \alpha)/(1+\alpha)} \right)^{1/2} - 1 \right) \tag{C4}$$

At times $t > t_e$, clump expansion is halted, and the clump is now confined by the pressure at the base of the PDR flow. The clump slowly loses mass, and shrinks to eventually become completely photoevaporated. The time evolution of clump mass and size can be obtained by differentiating equation (C3) which also holds for $t > t_e$, with respect to time and equating this with the mass loss rate (equation B11). Thus,

$$r_c(t > t_e) = r_c(t_e) - \frac{3}{2} c_{PDR} \frac{1+\alpha}{2\nu^2 + \alpha} (t - t_e), \tag{C5}$$

$$m_c(t > t_e) = m_{c0} \frac{2(2\nu^2 + \alpha)}{\eta_{c0}(1+\alpha)} \left(\frac{r_c(t)}{r_{c0}} \right)^2 . \tag{C6}$$

The photoevaporation timescale is obtained by setting the clump radius to zero at t_{PE} to give

$$t_{PE} = \left(\frac{2\nu^2 + \alpha}{1+\alpha} \right) \frac{r_c(0) + c_c t_e}{3 c_{PDR}} + t_e, \tag{C7}$$

and t_e is given by equation (C4).

D. Numerical hydrodynamics code

The fluid equations of motion for the system are solved using a 1-D spherical Lagrangian hydrodynamics code. The equations are solved using a finite difference method, with a numerical viscosity term, added as a pseudopressure, for accurate handling of shocks and discontinuities (Richtmyer & Morton 1967, Bowers & Wilson 1991). An isothermal equation of state is used throughout. The accuracy and stability of the scheme was checked with standard test problems with known solutions. The computational grid has 1000 equally spaced radial zones, except for the central 20%, which was spaced logarithmically in radius. This was done to increase spatial resolution at the centre, and it provides a more accurate calculation of any shock-induced collapse.

The FUV field is gradually turned on over a timescale, t_{FUV}, which is varied to accommodate both the impulsive and slow heating cases described in §4. The temperature of an outer shell of material is thus raised continuously from T_c to T_{PDR}, reaching its maximum value of the PDR temperature at a time t_{FUV}. The temperature T, exponentially drops off with the square of the column, N, into the cloud, $T(N) = T_c + (T_{PDR} - T_c)e^{-(N/N_0)^2}$. This

profile was chosen to closely mimic the T dependence with column predicted by PDR models for the values of G_0 and n under consideration (Kaufman et al. 1999).

REFERENCES

Allen, L. E., Burton, M.G., Ryder, S.D. et al. 1999, MNRAS, 304, 98

Bakes, E.L.O., & Tielens, A.G.G.M. 1994, ApJ, 427, 822

Bertoldi F., 1989, ApJ, 346, 735

Bertoldi F., Draine B. 1996, ApJ, 458, 222

Bertoldi F., McKee, C.F. 1990, ApJ, 354, 529

Bertoldi F., McKee, C.F. 1992, ApJ, 395, 140

Blitz, L. & Stark, A. 1986, ApJL, 300, 89

Blitz, L. 1991, The physics of star formation and early stellar evolution, Kluwer, p3

Block, D.L., Dyson, J.E., & Madsen, C. 1992, ApJ, 390, L13

Burton, M.G., Hollenbach, D.J., & Tielens, A.G.G.M. 1990, ApJ, 365, 620

Chandrasekhar, S. 1961, Hydrodynamic and hydromagnetic stability, Oxford:Clarendon Press

Crutcher, R.M. 1999, ApJ, 520, 706

Désert, F-X., Boulanger, F., Puget, J.L. 1990, A&A, 237, 215

Weingartner, J.C., & Draine, B.T. 2001, ApJS, 134, 263

Elmegreen, B.G. 1999, The Physics and Chemistry of the Interstellar Medium, p77

Evans, N.J., Davis, J.H., Mundy, L.G., & vandenBout, P. 1987, ApJ, 321, 344

Evans, N.J. 1999, ARA&A, 37, 311

Falgarone, E. & Phillips, T.G. 1990, ApJ, 359, 344

Genzel, R., 1991, Galactic Interstellar Medium, Saas-Fee Advanced Course 21 (Heidelberg:Springer-Verlag)

Goodman, A.A., Barranco, J.A., Wilner, D.J., & Heyer, M.H. 1998, ApJ, 504, 223

Habing, H.J. 1968, Bull. Astron. Inst. Netherlands, 19, 421

Henyey, L.C. & Greenstein, J.L. 1941, ApJ, 93, 70

Hill, J.K. & Hollenbach, D.J. 1978, ApJ, 225, 390

Hogerheijde, M.R., Janse, D.J., van Dishoeck, E.F. 1995, A&A, 294,792

Hollenbach D.J., Tielens A.G.G.M. 1999, Rev.Mod.Phys, 71,173

Howe, J.E., Jaffe, D.T., Genzel, R., & Stacey, G.J. 1991, ApJ, 373, 158

Hurwitz, M., Bowyer, S., & Martin, C. 1991, ApJ, 372, 167

Jijina, J., Myers, P.C., & Adams, F.C. 1999, ApJS, 125, 161

Johnstone D., Hollenbach D.J., Bally J. 1998, ApJ, 499, 758

Kaufman M.J., Wolfire M.G., Hollenbach D.J., Luhman M.L. 1999, ApJ, 527, 795

Klein R.I., McKee C.F., Colella P. 1994, ApJ, 420, 213

Kuchar, T.A., & Bania, T.M. 1993, ApJ, 414, 664

Luhman, K.L., Engelbracht, C.W., & Luhman, M.L. 1998, ApJ, 499, 799L

Maloney, P. 1988, ApJ, 334, 761

Marconi, A., Testi, L., Natta, A., Walmsley, C.M. 1998, A&A, 330, 453

McCaughrean, M.J. & Stauffer, J.R. 1994, AJ, 108, 1382

McKee, C.F. 1999, The Origins of Stars and Planetary Systems, eds. C.J. Lada, N.D.Kylafis, Kluwer, p29

Meixner, M., Haas, M.R., Tielens, A.G.G.M., Erickson, E.F. & Werner, M. 1992, ApJ, 390, 499

O'Dell, C.R., Wen, Z., Hu, X. 1993, ApJ, 410, 696

Oort, J.H., & Spitzer, L.J. 1955, ApJ, 121, 6

Parker, E.N. 1958, ApJ, 128, 664

Plume, R., Jaffe, D.T., Evans, N.J. et al. 1997, ApJ, 476, 730

Scalo, J. 1990, Physical processes in fragmentation and star formation, Kluwer, p151

Schneider, N., Stutzki, J., Winnewisser, G., Block, D. 1998, A&A, 335, 1049

Shu, F.H. 1977, ApJ, 214, 488

Steiman-Cameron, T.Y., Scargle, J.D., Imamura, J.N. & Middleditch, J. 1997, ApJ, 487, 396

Steiman-Cameron, T.Y., Hass, M., Tielens, A.G.G.M., & Burton, M.G. 1997, ApJ, 478, 261

Störzer H., Stutzki, J. & Sternberg, A. 1995, A&A, 296L, 9

Störzer H., Hollenbach D.J. 1999, ApJ, 515, 669

Störzer H., Hollenbach D.J. 1998, ApJ, 495, 853

Stutzki, J., Stacey, G.J., Genzel, R. et al. 1988, ApJ, 332, 379

Tauber, J., Tielens, A.G.G.M., Meixner, M., Goldsmith, P.F. 1994, ApJ, 422, 136

Tielens A.G.G.M., Hollenbach D.J 1985, ApJ, 291, 722

Tielens A.G.G.M., Hollenbach D.J 1985b, ApJ, 291, 747

van der Werf, P.P., Stutzki, J., Sternberg, A., Krabbe, A., 1996, A&A, 313,633

van der Werf, P., Goss, W.M., Heiles, C., Crutcher, R.M. & Troland, T.H. 1993, ApJ, 411, 247

Wang, Y., Jaffe, D.T., Evans, N.J. et al. 1993, ApJ, 419, 707

Ward-Thomson D., Kirk J.M., Crutcher R., Greaves J.S., Holland w.S., Andre P., 2000, ApJL, in press

Watson, W.D. 1972, ApJ, 176, 103

Whitworth, A.P. 1979, MNRAS, 186, 59

Williams, J.P., Blitz, L., & Stark, A.A. 1995, ApJ, 451, 252

Williams, J.P., Blitz, L., & McKee, C.F. 2000, Protostars and Planets IV, p97

Wyrowski, F., Walmsley, C.F., Goss, W.M., & Tielens, A.G.G.M. 2000, ApJ, 543, 245

Young Owl, R.C., Meixner, M., Wolfire, M., Tielens, A.G.G.M. 2000, & Tauber, J. ApJ, 540, 886

This preprint was prepared with the AAS LaTeX macros v5.0.

This figure "f3.jpeg" is available in "jpeg" format from:

http://arXiv.org/ps/astro-ph/0204180v1